Water Reuse

© 2022 The Authors

Water Reuse Vol 12 No 1, 131 doi: 10.2166/wrd.2022.001

Flat sheet metakaolin ceramic membrane for water desalination via direct contact membrane distillation

Tsegahun Mekonnen Zewdie [a,b,*], Nigus Gabbiye Habtu[a], Abhishek Dutta[c] and Bart Van der Bruggen[b]

[a] Faculty of Chemical and Food Engineering, Department of Chemical Engineering, Bahir Dar University, Bahir Dar, Ethiopia
[b] Department of Chemical Engineering, Faculty of Engineering, KU Leuven, Celestijnenlaan 200F, B-3001, Leuven, Belgium
[c] Department of Chemical Engineering, Izmir Institute of Technology, Gülbahçe Campus, Urla, Izmir 35430, Turkey
*Corresponding author. E-mail: tsegmek@gmail.com

TMZ, 0000-0003-3669-5257

ABSTRACT

Hydrophobic metakaolin-based flat sheet membrane was developed via phase inversion and sintering technique and modified through 1H,1H,2H,2H-perfluorooctyltriethoxysilane grafting agents. The prepared membrane was characterized by different techniques such as XRD, FTIR, SEM, contact angle, porosity, and mechanical strength. Their results indicated that the wettability, structural, and mechanical properties of the prepared membrane confirm the suitability of the material for membrane distillation (MD) application. The prepared metakaolin-based flat sheet membrane acquired hydrophobic properties after surface modification with the water contact angle values of 113.2° to 143.3°. Afterward, the membrane performance was tested for different sodium chloride aqueous solutions (synthetic seawater) and various operating parameters (feed temperature, feed flow rate) using direct contact membrane distillation (DCMD). Based on the findings, the prepared membrane at metakaolin loading of 45 wt.% and sintered at 1,300 °C was achieved the best performance with >95% salt rejection and permeate flux of 6.58 $\pm$ 0.3 L/m^2 · h at feed temperature of 80 °C, feed concentration of 35 g/L, and feed flow rate of 60 L/h. It can be concluded that further optimization of membrane porosity, mechanical, and surface properties is required to maximize the permeate flux and salt rejection.

Key words: desalination, direct contact membrane distillation, flat sheet, hydrophobic, metakaolin, phase inversion and sintering

HIGHLIGHTS

- The flat sheet ceramic membrane was synthesized for DCMD.
- The sintering process was a much more influential factor in the membrane shrinkage.
- The flat sheet ceramic membrane was successfully grafted with PFAS molecules.
- Effect of operating variable on the permeate flux and salt rejection.
- It was found that the feed temperature was the most significant operating variable affecting the performance of the DCMD.

GRAPHICAL ABSTRACT

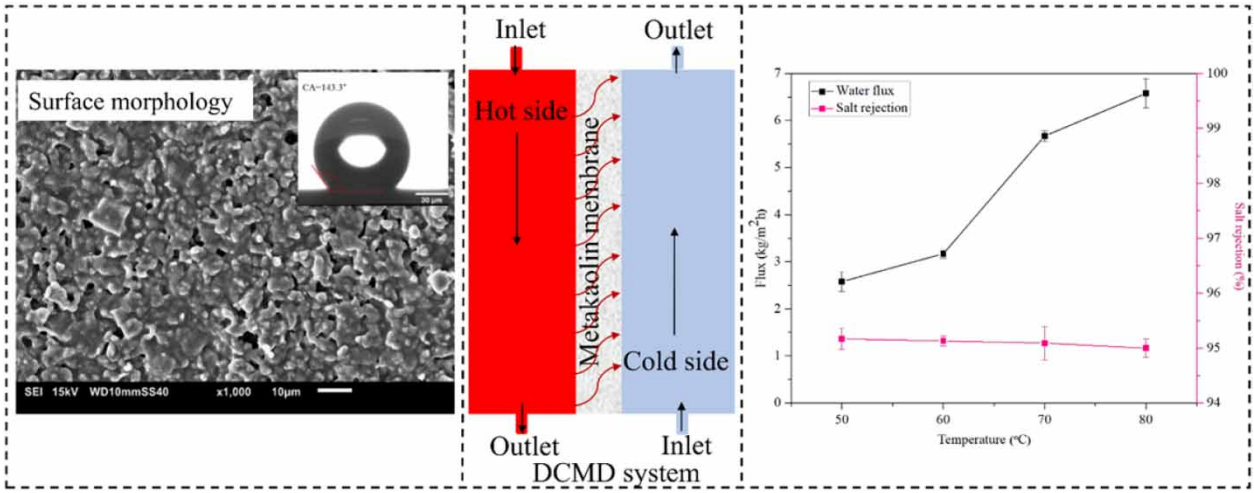

1. INTRODUCTION

Water is essential for all socio-economic development in many areas (Brusseau *et al.* 2019; Gomez *et al.* 2019). In recent years, the scarcity of safe and clean drinking water is among the main global challenges. This is due to higher standards of living, population growth, rapid industrial growth and advancement, and climate change (Brusseau *et al.* 2019; Kumari *et al.* 2021; Zulfiqar *et al.* 2021). To provide a sufficient amount of safe and clean drinking water, both thermal (non-membrane) and membrane-based water desalination techniques are required (Zewdie *et al.* 2021a). Thermal-based water desalination technologies include multi-effect distillation (MED), multistage flash (MSF) distillation, and vapor compression distillation (VCD) (Nafey *et al.* 2006; Baten & Stummeyer 2013; Gude 2018; Feria-Díaz *et al.* 2021). Membrane-based water desalination technologies include reverse osmosis (RO), electrodialysis (ED), pervaporation (PV), forward osmosis (FO), membrane distillation (MD), and hybrid membrane system (Sanmartino *et al.* 2016; Aliyu *et al.* 2018; Zewdie *et al.* 2021a). Membrane-based water desalination technologies are more energy-efficient, economic, and sustainable than thermal-based water desalination technologies (Baten & Stummeyer 2013; Roy & Ragunath 2018; Zewdie *et al.* 2021a). Among membrane-based water purification techniques, membrane distillation represents an emerging and promising approach for desalination and wastewater treatment application (Sanmartino *et al.* 2016; Alkhudhiri & Hilal 2018; Ashoor *et al.* 2018; Hussain *et al.* 2021; Saavedra *et al.* 2021; Tai *et al.* 2021). Membrane distillation is a hybrid separation technique combining thermal-driven distillation and membrane separation processes (Belessiotis *et al.* 2016; Ghaffour *et al.* 2019). Based on the type of configuration, membrane distillation is classified into direct contact membrane distillation (DCMD), sweeping gas membrane distillation (SGMD), vacuum membrane distillation (VMD), air gap membrane distillation (AGMD), and permeate gap membrane distillation (PGMD) (Gugliuzza & Basile 2013; Eykens *et al.* 2016a; Mahmoudi *et al.* 2018; Parani & Oluwafemi 2021).

Polymeric membranes (polypropylene (PP), polysulfone (PSF), polytetrafluoroethylene (PTFE), and polyvinylidene fluoride (PVDF)) (Shirazi *et al.* 2013; Ravi *et al.* 2020; Parani & Oluwafemi 2021) and ceramic membranes (alumina, titania, zirconia) have been widely studied for membrane distillation application (Hubadillah *et al.* 2019a; Bandar *et al.* 2021). As compared to polymeric membranes, ceramic membranes can withstand extreme conditions/harsh environments due to their excellent mechanical strength, biocompatibility, high thermal stability, high chemical stability, long lifetime, energy efficiency, availability, and sustainability (Fang *et al.* 2012; Arumugham *et al.* 2021). Ceramic membranes are known to have better antifouling and easy cleaning properties, which allows for repeated reuse (multiple uses) (Wang *et al.* 2018; Yang & Tang 2018). Ceramic membranes have the possibility to remove part of contamination (deposition and/or adsorption of solutes) from the pores by regeneration using various chemical agents (HCl, NaOH, NaClO, H_2O_2) and nano air bubbles (Hakami *et al.* 2020), however, the initial membrane performance and separation efficiency may not be restored (Kim & Jang 2016).

In this study, locally available and inexpensive Ethiopian kaolin was used as the primary raw material for the preparation of metakaolin-based flat sheet membranes. Some researchers prepared kaolin-based flat sheet membranes by various fabrication

methods such as combining phase inversion and sintering (Hubadillah *et al.* 2016a, 2018a), and dry pressing and sintering (Sahnoun & Baklouti 2013). Their results indicated that a thin flat sheet of kaolin-based membranes was difficult to handle during installation and application (Hubadillah *et al.* 2016a, 2016b, 2018a, 2018b). These negative consequences include easy break (brittleness) and high crack sensitivity features which have hindered a thin flat sheet of kaolin-based membranes for membrane distillation application. Thus, for addressing some of these shortcomings, the current study was proposed to develop metakaolin-based flat sheet membranes by phase inversion and sintering technique. Metakaolin is one type of calcined clay mineral and a well-known material for producing high mechanical strength (compressive and tensile strength) of silica-based ceramic membrane and, high-performance concretes (Dinakar *et al.* 2013; Hubadillah *et al.* 2016c; Khatib *et al.* 2018). A metakaolin-based flat sheet membrane is expected to be hydrophilic due to the presence of hydroxyl groups (OH) on its surface. This hydrophilicity is not suitable for the membrane distillation process (Kujawa *et al.* 2014a, 2016; Hubadillah *et al.* 2019a; Twibi *et al.* 2021). To improve the hydrophobicity of a ceramic membrane, it is necessary to modify the surface of membranes. There are three ways commonly used methods of surface modification of polymeric and ceramic membrane, which are chemical modification, surface morphology modification, and combination of chemical and morphology modifications (Khemakhem *et al.* 2013, 2014; Usman *et al.* 2021). Among these methods, grafting with perfluoroalkylsilanes (PFAS) is the most commonly applied, especially in membrane distillation applications, because the molecules of the modifiers are covalently attached to the surface as well as inside the porous structure of the ceramic membranes/materials (Kujawa *et al.* 2014a, 2014b, 2016; Abu-Zeid *et al.* 2015; Zuo & Chung 2016; Hubadillah *et al.* 2019a; Twibi *et al.* 2021).

This study aims to fabricate a metakaolin-based flat sheet membrane by combining phase inversion and sintering techniques for water desalination via DCMD. The main purpose of this study was to investigate the effect of metakaolin content and sintering temperature on the surface morphology, porosity, hydrophobicity property, and mechanical strength of the eventual metakaolin-based flat sheet membrane. This is the first broader study on the use of modified metakaolin-based flat sheet ceramic membranes in the membrane distillation process.

2. MATERIALS AND METHODS

2.1. Raw materials

Beneficiated and calcined Ethiopia kaolin (metakaolin) powder from our previous study (Zewdie *et al.* 2021b) was used as the ceramic material. Analytical grade polyethersulfone (PES; Radel 3100P, Solvay Advanced Polymer), polyethyleneglycol-30 dipolyhydroxystearate (Arlacel P135, CRODA, Belgium), and *N*-methyl-2-pyrrolidone (NMP; VWR International bvba, Belgium) were purchased and used as a polymer binder, dispersant, and solvent, respectively. Deionized water was used as the non-solvent coagulation bath. 1H,1H,2H,2H-perfluorooctyltriethoxysilane (PFAS; 97%, VWR International bvba, Belgium) was used as a grafting agent, and ethanol (>99.8%, Sigma-Aldrich, Belgium), acetone, and alkaline solution (NaOH at pH 10).

2.2. Fabrication of metakaolin flat sheet membrane

The preparation of metakaolin-based flat sheet membrane was conducted at four different metakaolin contents with four different sintering temperatures (1,200, 1,300, 1,400, and 1,500 °C) (Figure 1). The detailed compositions of the dope solutions are listed in Table 1.

Beneficiated and calcined kaolin (metakaolin) powder and PES were dried to ensure that no moisture was trapped in the particle. Then, the required quantity of NMP was taken in a 250 ml glass bottle and PES was slowly added and stirred by a hot plate magnetic stirrer for 4 h under continuous moderate stirring (300 rpm) to form the polymer solution. Arlacel P135 was then added as a dispersant into a polymer solution and stirred by a hot plate magnetic stirrer for 24 h under continuous moderate stirring (300 rpm). After the polymer solution was formed, metakaolin powder was then added into a polymer solution slowly and then stirred by a hot plate magnetic stirrer for 72 h under continuous moderate stirring (300 rpm) at 60 °C to ensure that the metakaolin powder and polymer solution were mixed well. The resulting dope solution was degassed in an ultrasonic bath for 30 min at room temperature to eliminate the air bubbles. The casting dope solution was cast on a casting machine and left for the evaporation process to occur for 30 s before the solvent exchange in the coagulation bath. The cast slurry was left in the water bath (2 L deionized water) for 24 h to let the phase inversion process be completed. Afterward, the membrane precursors were dried at room temperature for 24 h. Before the sintering process, the membrane precursors were cut in a square form (100 mm × 100 mm). The membrane precursors were then placed in an electric furnace and

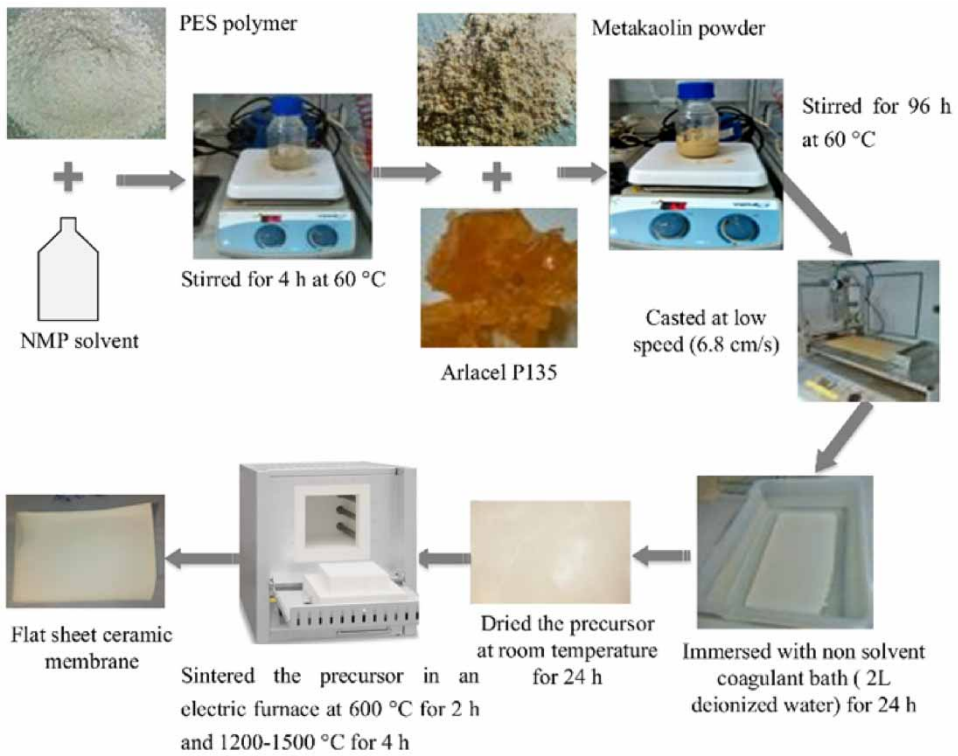

Figure 1 | Schematic diagram of metakaolin-based flat sheet membrane fabrication using phase inversion and sintering techniques.

Table 1 | Composition of the ceramic suspensions with different metakaolin contents

Membranes	1	2	3	4
Metakaolin (wt.%)	37.5	40	42.5	45
NMP (wt.%)	56.5	54	51.5	49
PES (wt.%)	5	5	5	5
Arlacel P135 (wt.%)	1	1	1	1

sintered in a controlled furnace to 600 °C at a rate of 2 °C min^{-1} and held for 2 h, then to target temperature (1,200, 1,300, 1,400, and 1,500 °C) at a rate of 5 °C min^{-1} and held for 4 h. Lastly, the furnace was cooled down at a rate of 5 °C min^{-1} to room temperature.

2.3. Preparation of hydrophobic metakaolin-based flat sheet membrane

Metakaolin-based membranes are hydrophilic. Hydrophilic membranes are not suitable to be used for membrane distillation applications (Hubadillah *et al.* 2019a; Twibi *et al.* 2021). Thus, surface modification/grafting is required to obtain hydrophobic properties. Four equal size metakaolin-based flat sheet membranes prepared at various sintering temperatures (1,200, 1,300, 1,400, and 1,500 °C) were used for this treatment. The membranes were cleaned using ethanol, acetone, and distilled water for 10 min, respectively. The samples were dried in an oven at 105 °C for approximately 12 h and have been treated by using an alkaline solution (NaOH at pH 10) for 8 h.

The treated samples were completely immersed and soaked into a 2 wt.% FAS (1H,1H,2H,2H-perfluorooctyltriethoxysilane) in ethanol solution for different grafting times (12, 24, 48, 72, and 96 h) to allow the coupling reaction to occur. Then, the grafted membranes were then rinsed with ethanol, acetone, and distilled water successively and dried at 105 °C for 12 h in an oven. The modified membranes have been characterized using different methods such as contact angle measurement (Kruss DSA 10Mk2, Germany), Fourier Transform Infrared Spectroscopy (FTIR; Perkin Elmer Spectrum

100, USA), and Scanning Electronic Microscopy (SEM; JEOL, JSM-6010LV, Tokyo, Japan) to determine the grafting efficiency. Also, the grafting degree (GD) was calculated by Espiritu *et al.* (2016), Hernández-Aguirre *et al.* (2016), and Lim & Shin (2020).

$$\mathrm{GD}(\%) = \frac{(W_\mathrm{f} - W_\mathrm{b})}{W_\mathrm{b}} \times 100 \tag{1}$$

where W_b and W_f are the mass of the metakaolin-based membrane before and after modification, respectively.

2.4. Characterization of membranes

The identification of the crystalline phases was carried out by X-Ray Diffraction (XRD; D2 phaser, Bruker, Germany) using Cu-Kα1 radiation at a scanning rate of 2° min^{-1}. Fourier Transform Infrared (FTIR) spectroscopy (Perkin Elmer Spectrum 100, USA) over the range of 4,000–400 cm^{-1} was used to measure the surface properties of ceramic membrane before and after grafting. Membrane thickness was measured using a digital micrometer (0–25 mm, Fowler IP54) measure at different spots at least 10 times, and the average value was reported. Furthermore, the structure of the metakaolin-based membrane was examined using an SEM (JEOL, JSM-6010LV, Tokyo, Japan). The metakaolin-based membrane samples were cut into 5 mm × 5 mm size and placed on a metal holder, which was then sputtered by platinum under vacuum before testing. The images of the metakaolin-based membrane were captured to examine the overall view and porous structure of the metakaolin-based membrane at different metakaolin contents: 37.5, 40, 42.5, and 45 wt.%. The contact angle of metakaolin-based membranes sintered to different final temperatures ranging from 1,200 to 1,500 °C were measured by the sessile drop method (Kruss DSA 10Mk2, Germany) using distilled water at room temperature. All contact angle readings were taken 10 min after a 0.5 ml water droplet was placed on the membrane surface. Thermal conductivity (C-Therm TCi Thermal Conductivity Analyzer, Canada) of the metakaolin-based membrane was measured using MTPS (ASTM D7984) method with a water contact agent (0–70 °C). The shrinkage percentage that occurred during the sintering process was determined using the dimensions (volume) of the flat green ceramic specimen before and after being sintered at a temperature range of 1,200–1,500 °C. The total linear shrinkage percentage of the metakaolin-based flat sheet membrane was determined by Zulkifli *et al.* (2020).

$$\text{Total linear shrinkage} = \left(\frac{V_0 - V_f}{V_o}\right) \times 100 \tag{2}$$

The mechanical strength of the sample was determined by the three-point bending strength method. The three-point bending test was carried out with a dynamic mechanical analysis (DMA; Model Q800, TA Instruments, USA) machine. The bending strength (σ_b) of a flat sheet sample was calculated by Hara *et al.* (2014) and Obada *et al.* (2017a).

$$\sigma_\mathrm{b} = \frac{3FL}{2Wt_\mathrm{m}^2} \tag{3}$$

where σ_b is bending strength, F is fracture force, L is membrane support span length, W is membrane support width, and t_m is membrane support thickness.

Archimedes' principle was used for the prepared membrane porosity determination. For this purpose, firstly, the membrane was dried at 105 °C for 12 h and weighed to obtain its dry weight followed by weighing after immersion in distilled water for about 24 h and then removing extra water on the membrane surface by a tissue paper to measure its wet weight. The porosity of the prepared membrane was calculated by Abd Aziz *et al.* (2019).

$$\text{Porosity} = \left(\frac{(W_w - W_d)/\rho_w}{V_\mathrm{mem}}\right) \times 100 \tag{4}$$

2.5. DCMD test

An experimental laboratory-scale DCMD setup was constructed with an effective membrane area of 0.0025 m^2 (50 mm × 50 mm) located in a plate and frame (flat sheet membranes) module made of Plexiglas™ with 90 mm × 90 mm dimensions. The desalination performance of metakaolin-based flat sheet membranes in different operating conditions including feed inlet

temperature, feed inlet flow rate, feed inlet concentration under counter-current flow pattern was investigated. The membrane had an approximate thickness of 400 μm and exhibit low values of effective thermal conductivity. The membrane cell consisted of two compartments, the feed side and the permeate side. Figure 2 shows the experimental setup.

The synthetic solutions were prepared by dissolving a reagent grade NaCl salt (supplied by Fluka) in distilled water to obtain different salt concentrations (0, 5, 15, 25, and 35 g/L) and served as the feed solution on the hot side of the module. The feed container was immersed in a water bath and heated until it reaches a predetermined operating temperature (50, 60, 70, and 80 °C). The hot feed was circulated with a peristaltic pump (Model, Sci-Q 323) into the membrane module with a flow rate of 30, 40, 50, and 60 L/h. A coiled heater was used to regulate the temperature of the hot stream. Deionized water was used as a cooling liquid on the permeate side of the module from a double-walled cooling water container by a peristaltic pump (Model, Sci-Q 323) at a constant flow rate of 40 L/h. A cooling thermostat was used to regulate the temperature of the cold stream.

The inlet temperatures of the hot feed and the cold water were measured by two digital thermometers (Model, HI98509 Checktemp®1). The electrical conductivity or the salt concentration of the feed and permeate solution was measured by a conductivity meter (Radiometer CDM230, Sweden) inserted into the vessel. After the flow rates of the hot solution, cold distillate water, and the two inlet and outlet temperatures were stabilized, it was assumed that the experimental conditions had reached a steady state; the permeated liquid was circulated through a double-walled cooling water reservoir, and the volume measured at regular intervals was used to calculate the water vapor flux through the membrane under the given experimental conditions.

The water vapor flux of the membrane distillation membrane was calculated and expressed in J (kg/m^2 h) (Hubadillah *et al.* 2018b; Abd Aziz *et al.* 2019; Mohamed Bazin *et al.* 2019; Abdelrazeq *et al.* 2020; Tai *et al.* 2021).

$$\text{Water vapor flux } (J) = \frac{V_w \times \rho_w}{A \times t} \tag{5}$$

where V_w is the volume of water transferred (L), ρ_w is the density of water (kg/L), A is the effective membrane area (m^2), and t is the time required to collect a certain amount of permeate (h). DCMD experiments were repeated three times, and the average flux value was calculated to narrow the error range.

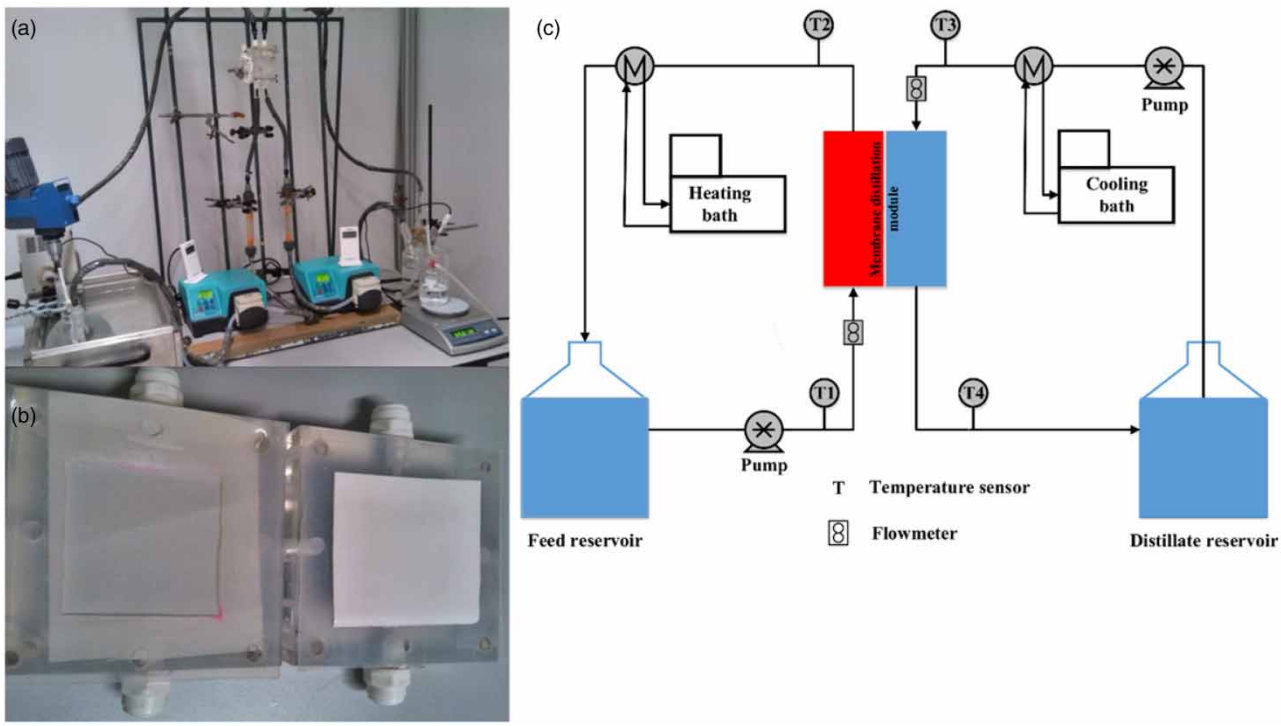

Figure 2 | (a) Laboratory-scale membrane distillation setup; (b) flat sheet direct contact membrane distillation module; and (c) scheme of the membrane distillation setup.

The salt rejection (R) of the membrane distillation membrane was determined by Li *et al.* (2015), Hubadillah *et al.* (2018b), and Tai *et al.* (2021):

$$\text{Rejection (\%)} = \frac{C_f - C_p}{C_f} \times 100 \quad (6)$$

where C_f is the salinity in the feed solution (μs/cm) and C_p is the salinity of the permeate solution (μs/cm).

3. RESULTS AND DISCUSSION

3.1. Characterization of starting materials and membranes

The physical properties of beneficiated Ethiopian kaolin and beneficiated and calcined kaolin (metakaolin) were reported in previous work (Zewdie *et al.* 2021b). Powder particle size and the distribution of the starting material (raw material) are critical factors in the fabrication of ceramic membranes (Hubadillah *et al.* 2016a; Al-Naib 2018). According to the literature, the powder particle size used in the fabrication of ceramic membrane is mainly in the range of 1 μm (Harabi *et al.* 2014; Hubadillah *et al.* 2019b) to 15 μm (Zhou *et al.* 2010). In this study, the particle size of beneficiated and calcined kaolin (metakaolin) is sufficiently small suggesting its suitability for ceramic membrane fabrication. The powder particle size and the distribution affected the viscosity of the ceramic suspension, the movement of the particles in ceramic suspension during phase inversion, and the particle migration and bindings during sintering at high temperatures (Konijn *et al.* 2014; Renteria *et al.* 2019; Li *et al.* 2020a). Moreover, powder particle size and the distribution of the starting material (raw material) affected the morphology characteristic and the porosity of the fabricated ceramic membrane (Hubadillah *et al.* 2016a, 2021; Ji *et al.* 2020).

3.2. XRF analyses

The chemical composition of beneficiated Ethiopian kaolin and beneficiated and calcined kaolin (metakaolin) were reported in previous work (Zewdie *et al.* 2021b). The analysis showed that the composition of SiO_2 and Al_2O_3 varied between 60.10 and 60.30%, and 27.60 and 29.40%, respectively. On the other hand, the loss on ignition varied between 10.7 and 0.98%. These amounts were close to the values determined for theoretical kaolin and metakaolin. Due to its lower iron oxide content and SiO_2/Al_2O_3 mass ratio, and higher Al_2O_3/Fe_2O_3 mass ratio, beneficiated and calcined kaolin (metakaolin) is a suitable cheap raw material for developing ceramic membranes for water purification.

3.3. XRD measurements

Figure 3 presents the XRD patterns of beneficiated Ethiopia kaolin, beneficiated and calcined kaolin (metakaolin), and metakaolin-based flat sheet membrane. It can be noted that the XRD patterns of beneficiated Ethiopia kaolin, beneficiated and calcined kaolin (metakaolin) powder, and metakaolin-based flat sheet membrane reported in Figure 3 depict a clear difference. During the calcination process, the kaolinite structure is disordered due to dihydroxylation (Cheng *et al.* 2019; Izadifar *et al.* 2020). Due to this, the complex structural transformation of kaolinite mullite is formed. As shown in the previous study (Zewdie *et al.* 2021b), XRD peaks at Bragg's angles of 12.4°, 25.1°, 32.2°, 40.5°, and 44.1° represented the presence of kaolinite minerals in beneficiated Ethiopian kaolin powder. Similar trends have been reported elsewhere (Djobo *et al.* 2014; Douiri *et al.* 2017; Khan *et al.* 2017; Obada *et al.* 2017b) for other types of clay used in ceramic membrane fabrication. During the sintering process, kaolinite peaks disappeared whereas mullite ceramic peaks were formed in all XRD patterns for metakaolin-based flat sheet membrane (Sahnoun & Baklouti 2013; Abdulhameed *et al.* 2017a, 2017b; Obada *et al.* 2017b). The XRD patterns showed that by increasing the sintering temperature from 1,200 to 1,500 °C, the peak intensity of mullite ceramic became stronger which indicated that the amount of mullite increased with increasing sintering temperature (Chen *et al.* 2008; Abdulhameed *et al.* 2017a, 2017b; Mohtor *et al.* 2017; Liu *et al.* 2021; Ndjigui *et al.* 2021). Besides that, XRD peaks at Bragg's angles of 27.3°, 27.5°, and 60.6° were also observed in beneficiated Ethiopian kaolin, beneficiated and calcined kaolin (metakaolin) powder, and metakaolin-based flat sheet membrane, respectively, which indicated the presence of non-clay mineral (quartz). XRD analysis revealed a significant predominance of quartz and kaolinite in the beneficiated Ethiopian kaolin clay. These observations are in agreement with the X-ray fluorescence (XRF) results in the previous study (Zewdie *et al.* 2021b). It has also been noticed that the beneficiated Ethiopian kaolin powder used in this study consisted of quartz as the non-clay mineral in which the XRD peaks remained for metakaolin-based flat sheet membranes sintered at different target temperatures (1,200–1,500 °C) (Sahnoun & Baklouti 2013; Mohtor *et al.* 2017; Magalhaes *et al.*

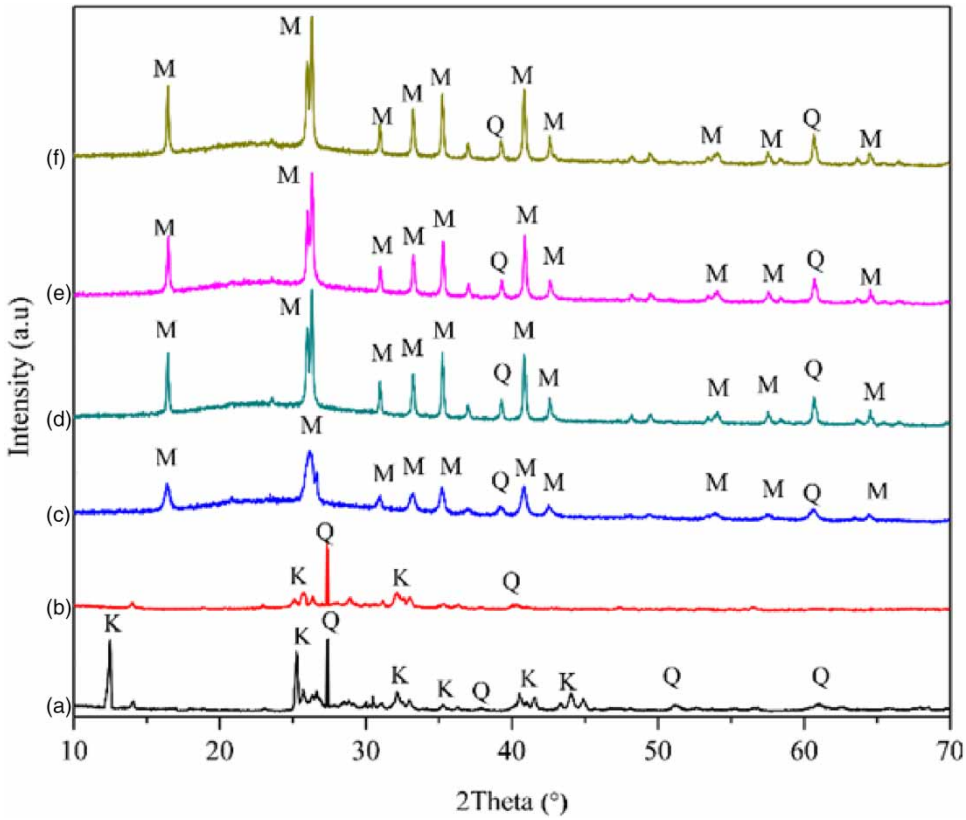

Figure 3 | XRD patterns of (a) beneficiated Ethiopian kaolin, (b) beneficiated and calcined kaolin (metakaolin) powder, and metakaolin-based flat sheet membranes (45 wt.% metakaolin loading) sintered at (c) 1,200 °C, (d) 1,300 °C, (e) 1,400 °C, and (f) 1,500 °C (K: kaolinite; Q: quartz; M: mullite).

2020). According to the XRD analysis, it was also proved that the higher sintering temperature has no dramatic change on the mullite phase presented in metakaolin-based flat sheet membrane (Figure 3). Additionally, the intensity of the XRD peaks of quartz decreased with temperature (Mohamed Bazin *et al.* 2019; Magalhaes *et al.* 2020).

3.4. TGA/DSC analyses

The TGA/DSC is an important analysis that needs to be performed on the powder samples. As shown in the previous study (Zewdie *et al.* 2021b), TGA/DSC curves were obtained from the simultaneous thermal analysis of the beneficiated Ethiopian kaolin and beneficiated and calcined kaolin (metakaolin) powder. The total weight loss of mass was 9.12 wt.% for beneficiated Ethiopian kaolin and 0.55 wt.% for beneficiated and calcined kaolin (metakaolin). The TGA/DSC analysis has proven that the thermal properties of beneficiated Ethiopian kaolin and beneficiated and calcined kaolin (metakaolin) powders are suitable for possible industrial use, especially for ceramic membrane fabrication.

3.5. FTIR measurements

FTIR spectra of the beneficiated Ethiopia kaolin powder, beneficiated and calcined kaolin (metakaolin) powder, and metakaolin-based flat sheet membrane are shown in Figure 4. According to the result presented in Figure 4(a), beneficiated Ethiopia kaolin powder has OH-bending modes at 1,122 cm^{-1} and OH-stretching modes at 3,619 and 3,688 cm^{-1} (Khan *et al.* 2017; Mohtor *et al.* 2017; Boussemghoune *et al.* 2020). Moreover, the absorption band at around 1,626 cm^{-1} was observed in beneficiated Ethiopia kaolin powder due to its deformation vibration of physisorbed water molecules at the surface (Khan *et al.* 2017; Kljajević *et al.* 2017; Aragaw & Angerasa 2020). The absorption band for beneficiated Ethiopia kaolin powder at 920 cm^{-1} was attributed to Al–OH bending vibration (Aragaw & Angerasa 2020). This sharp band disappeared in all spectra of beneficiated and calcined kaolin (metakaolin) powder and metakaolin-based flat sheet membranes as a result of the bonds breaking between the octahedral sheet and tetrahedral sheet of kaolinite structure due to the mullitization process

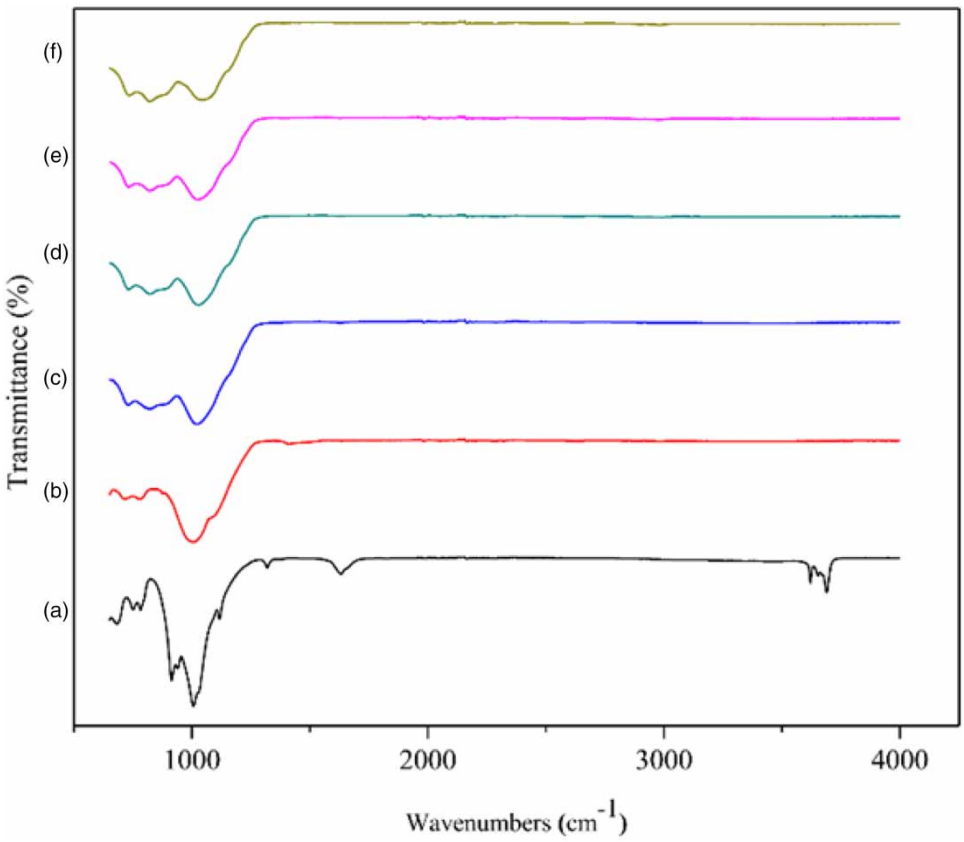

Figure 4 | FTIR spectra of (a) beneficiated Ethiopia kaolin powder, (b) beneficiated and calcined kaolin (metakaolin) powder, and flat sheet membranes (45 wt.% metakaolin loading) sintered at (c) 1,200 °C, (d) 1,300 °C, (e) 1,400 °C, and (f) 1,500 °C.

of kaolinite at a high sintering temperature and for a long sintering time (Mohtor *et al.* 2017). Beneficiated and calcined kaolin (metakaolin) powder and metakaolin-based flat sheet membranes sintered at different temperatures do not contain OH because of the loss of structural hydroxyl group due to the sintering process. As a result of the sintering process, these characteristic bands for kaolinite structure diminished in all spectra of metakaolin powder and metakaolin-based flat sheet membranes, showing that the sintering process was adequate for complete dehydroxylation and structural distortion of kaolinite and its transformation into metakaolin (Mohtor *et al.* 2017; Merabtene *et al.* 2019; Magalhaes *et al.* 2020).

The band between 900 and 1,150 cm^{-1} is relatively wide in beneficiated and calcined kaolin (metakaolin) powder, but in metakaolin membranes sintered at different temperatures, it becomes a relatively narrow band which explains the strong bond of aluminosilicate molecules in metakaolin membranes resulting in the increase of its mechanical strength.

3.6. Morphological properties of membranes

During the phase inversion process, shrinkage of the flat sheet precursor occurred (Bikel *et al.* 2010; dan Sinteran 2017). This is because the rate of solvent (NMP) diffusion from the suspension is always faster than the rate of diffusion of water into the suspension (Bonyadi *et al.* 2007; dan Sinteran 2017). Similarly, during the sintering process, organic components (polymer binders) were removed from the precursors, and only inorganic mineral was left in the metakaolin-based membranes after the sintering process (Wang *et al.* 2009; Paiman *et al.* 2015). Then, the shrinkage of the metakaolin-based flat sheet membrane was determined using dimensions (volume) of the membrane before and after sintering. Figure 5 depicts the percentage of shrinkage volume for the metakaolin-based flat sheet membrane sintered at a targeted temperature (1,200–1,500 °C) in different beneficiated and calcined kaolin (metakaolin) contents (37.5–45 wt.%). The maximum shrinkage of the volume for the metakaolin-based flat sheet membrane sintered at a targeted temperature of 1,200, 1,300, 1,400, and 1,500 °C in 45 wt.% metakaolin is found to be 10.31 $\pm$ 4.25%, 31.24 $\pm$ 3.74%, 46.97 $\pm$ 1.42%, and 53.93 $\pm$ 0.21%, respectively.

The more the shrinkage, the higher the internal stress generation, which results in more shape distortions and severe cracks or warps in the final sintered ceramic membrane (Green *et al.* 2008; Ni *et al.* 2013). This is due to the internal rearrangement

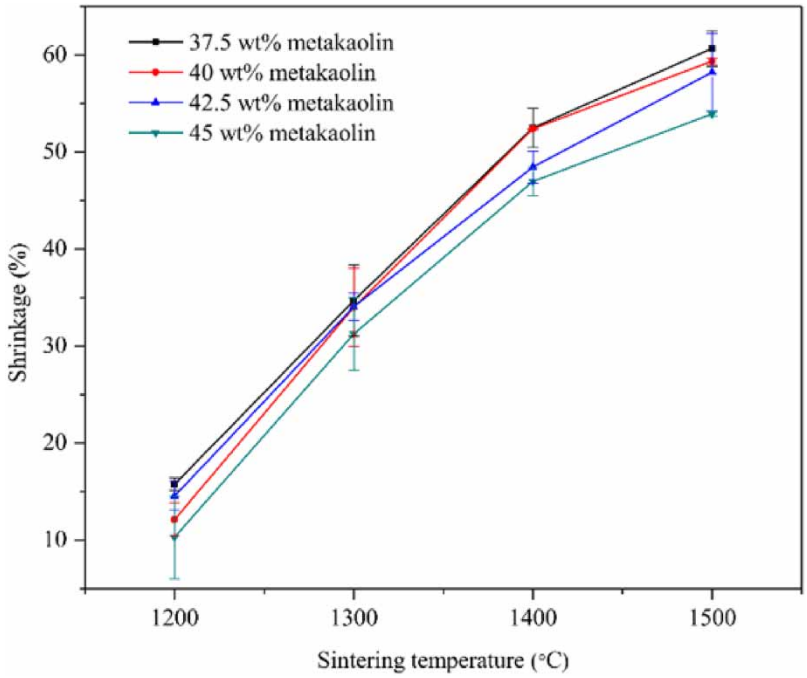

Figure 5 | Volume shrinkage of the flat sheet metakaolin-based membrane at a targeted sintering temperature (1,200–1,500 °C) in different metakaolin contents (37.5–45 wt.%).

(densification process) of the membrane at a higher temperature. It can be concluded that the shrinkage of the metakaolin-based flat sheet membrane increases with the sintering temperature. Similar results have been reported in previous studies (Qiu *et al.* 2009; Vasanth *et al.* 2011; Mankai *et al.* 2018; Elgamouz *et al.* 2019; Jiang *et al.* 2019; Li *et al.* 2020b; Ndjigui *et al.* 2021; Souza *et al.* 2021) for clay materials used in ceramic membrane fabrication. These results indicate that the metakaolin-based flat sheet membrane is suitable for application in DCMD for water desalination (Eykens *et al.* 2016b).

3.7. Evaluating the grafting efficiency

After chemical modification, the grafting efficiency of the flat sheet metakaolin-based ceramic membranes was determined by measurement of grafting degree and contact angle measurement.

3.8. Degree of grafting

The dependence of grafting time on grafting degree with membrane sintered at different sintering temperatures (1,200, 1,300, 1,400, and 1,500 °C) was evidenced in Figure 6. The grafting process was carried out at room temperature at different grafting times (12, 24, 48, 72, and 96 h). The grafting degree of the reaction system could change for membranes sintered at different sintering temperatures. The grafting degree of metakaolin-based membrane sintered at 1,200 °C was 3.25 $\pm$ 0.1%, 3.43 $\pm$ 0.25%, 3.94 $\pm$0.13%, 4.6 $\pm$ 0.06%, and 4.03 $\pm$ 0.14% corresponding to a reaction time of 12, 24, 48, 72, and 96 h, respectively. As shown in Figure 6, the grafting efficiency is proportional to the grafting time, where the modified membranes presented the highest grafting degree at 72 h. The determined grafting degree values for metakaolin-based membrane increased with grafting time from 12 to 72 h. Thus, the longer membrane hydrophobization leads to the creation of a smoother surface (lower surface roughness). The membrane also has a high contact angle due to a higher level of PFAS grafting agent concentration and covering all active sites on the membrane surface (Kujawa *et al.* 2016; Li *et al.* 2021). For a grafting time longer than 72 h, the value of grafting degree was slightly lower. This is due to a long-time interaction between the hydroxyl group on the metakaolin-based ceramic membrane surface and Si–O-alkyl groups of the PFAS grafting agent, which contributes to a decline in the amount of hydroxyl group. This is associated with the fact that contact angle increases with increasing the grafting time from 12 to 72 h, while it decreases with increasing grafting time longer than 72 h (Lu *et al.* 2009). Furthermore, it can be seen that a membrane sintered at a lower temperature leads to a higher grafting degree (Figure 6). A similar grafting process was also found in the literature for ceramic membrane (Lu *et al.* 2009; Fang *et al.*

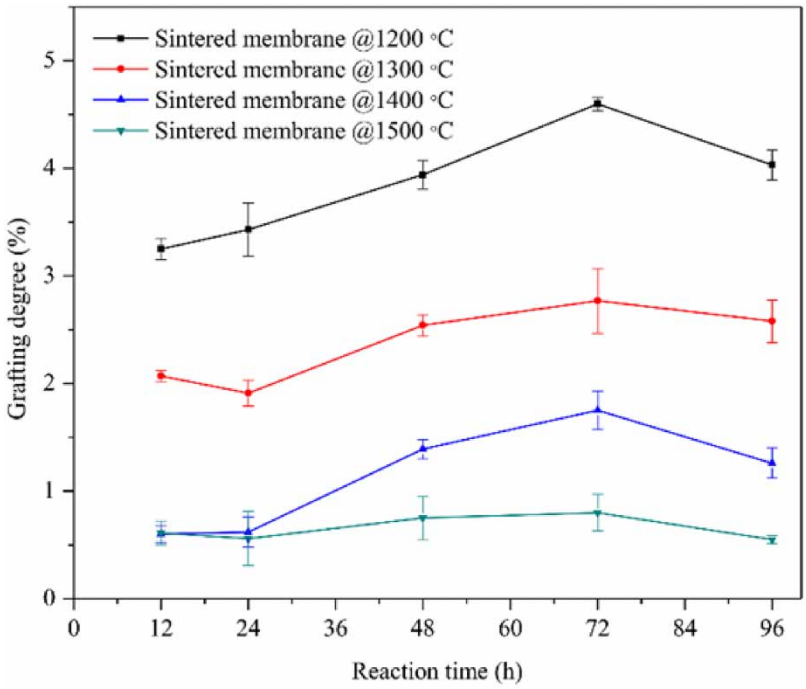

Figure 6 | Effect of reaction time on grafting degree of the metakaolin-based membrane (45 wt.% metakaolin loading) sintered at 1,200 °C, 1,300 °C, 1,400 °C, and 1,500 °C.

2012; Kujawa *et al.* 2013, 2014b, 2016; Hubadillah *et al.* 2019c; Saud *et al.* 2021) and clay powder materials (Kujawa *et al.* 2014b, 2014c).

3.9. Contact angle measurements

It was shown that the hydrophilic property of a metakaolin-based flat sheet membrane could be changed into a hydrophobic one by grafting 1H,1H,2H,2H-perfluorodecyltriethoxysilane on the surface of a metakaolin-based flat sheet membrane. The grafting process can be performed by a reaction between OH^- groups on the ceramic membrane surface and Si-O-alkyl groups of the silane (Krajewski *et al.* 2006; Khemakhem & Amar 2011; Khemakhem *et al.* 2014; Wang *et al.* 2016; Zuo & Chung 2016; Yang *et al.* 2017; Twibi *et al.* 2021). The surface modifying process can decrease the surface free energy and increase the contact angle of the membranes (Kujawa *et al.* 2017; Shahabadi *et al.* 2017; Yang *et al.* 2017; Hubadillah *et al.* 2018c; Dong *et al.* 2020). During the sintering process at temperatures between 400 and 800 °C, the hydroxyl groups (OH^-) can be suppressed from the membrane surface. Therefore, alkaline pretreatment is required to restore hydroxyl groups (OH^-) on the membrane surface and allow more coupling reactions with PFAS. Water drops deposited on the non-grafted metakaolin-based flat sheet membrane form a contact angle of $3.6 \pm 0.37°$ (super hydrophilic) (Figure 7(a)). This is

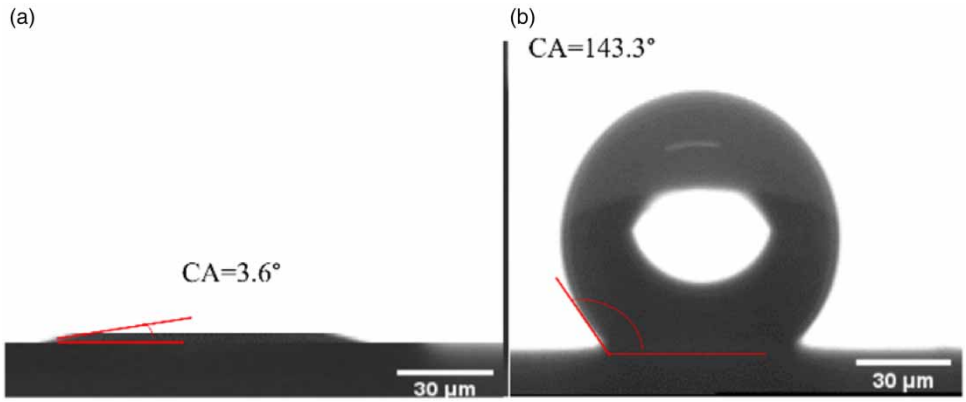

Figure 7 | The water contact angle of the membrane surface: (a) before grafting and (b) after grafting.

due to the uniform distribution of hydroxyl groups on the membrane surface. After grafting, the contact angle for grafted metakaolin-based flat sheet membrane sintered at a temperature of 1,200 °C was 143.3 ± 0.5°, proving that the metakaolin-based flat sheet membrane surface was successfully changed into superhydrophobic (Figure 7(b)) by grafting with PFAS. These results adequately demonstrate that the modified metakaolin-based flat sheet membrane is hydrophobic and sufficient for application in the DCMD for water desalination (Khayet 2011; Liu *et al.* 2012; Ren *et al.* 2015; Yang *et al.* 2017). Contact angle values of modified membranes were higher than for unmodified membranes, which indicate that grafting the membrane surface revealed a highly hydrophobic character. Similar phenomena have been observed in previous studies (Kujawa *et al.* 2014a; Wang *et al.* 2016; Yang *et al.* 2017; Hubadillah *et al.* 2018c, 2019c; Polak *et al.* 2021; Saud *et al.* 2021; Twibi *et al.* 2021).

The contact angle measurement of metakaolin-based membranes sintered at different targeted temperatures (1,200, 1,300, 1,400, and 1,500 °C) before and after chemical modification is shown in Figure 8. After grafting, the pore size of the membrane sintered at 1,200 °C became smaller due to PFAS grafted on the metakaolin-based flat sheet membrane surface. The highest hydrophobicity value was obtained by grafted metakaolin-based flat sheet membrane sintered at 1,200 °C with a contact angle value of 143.3 ± 0.5°. This was subsequently described as grafted metakaolin-based flat sheet membrane sintered at 1,200 °C that obtained a microtextured or micropatterned surface as shown in the SEM images (Figure 9).

3.10. SEM measurements

The effect of sintering temperature (ranging from 1,200 to 1,500 °C) on the membrane surface morphology of metakaolin-based flat sheet membrane before and after grafting was investigated by SEM, and corresponding images are shown in Figure 9. The SEM results indicated that no cracks were present in any membranes. The surface morphology of the membrane was found to be uniform and free of any defect. The porous structure and uniformly distributed pore were observed in the sintered membrane at 1,200 °C. The SEM results indicated that the membranes were cast from 45 wt.% metakaolin loading and sintered at 1,200 °C have a higher porosity than the membranes sintered at 1,500 °C. The increase in sintering temperature of the membranes has decreased the porosity of the membrane, from 40.28 ± 0.93% to 14.50 ± 1.89% for temperatures from 1,200 to 1,500 °C, respectively. Thus, the SEM micrographs reported in Figure 9 show that the effect of sintering is very marked; a progressive reduction of porosity can be observed when temperature increases. The number of pores decreased when the sintering temperature increased. At higher sintering temperatures, small pores disappeared and a less porous structure was produced, where sintering at 1,500 °C produced the strongest membrane with a highly dense structure and limited grain and non-interconnected pores. This may be due to the particles binding/aggregating together and it forms a dense

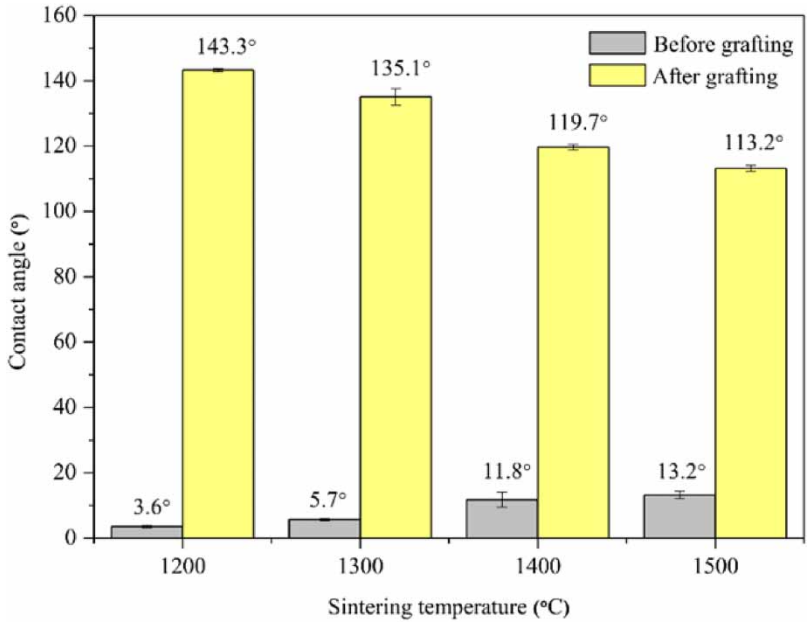

Figure 8 | The contact angle of a metakaolin-based membrane (45 wt.% metakaolin loading) surface: (a) before grafting and (b) after grafting.

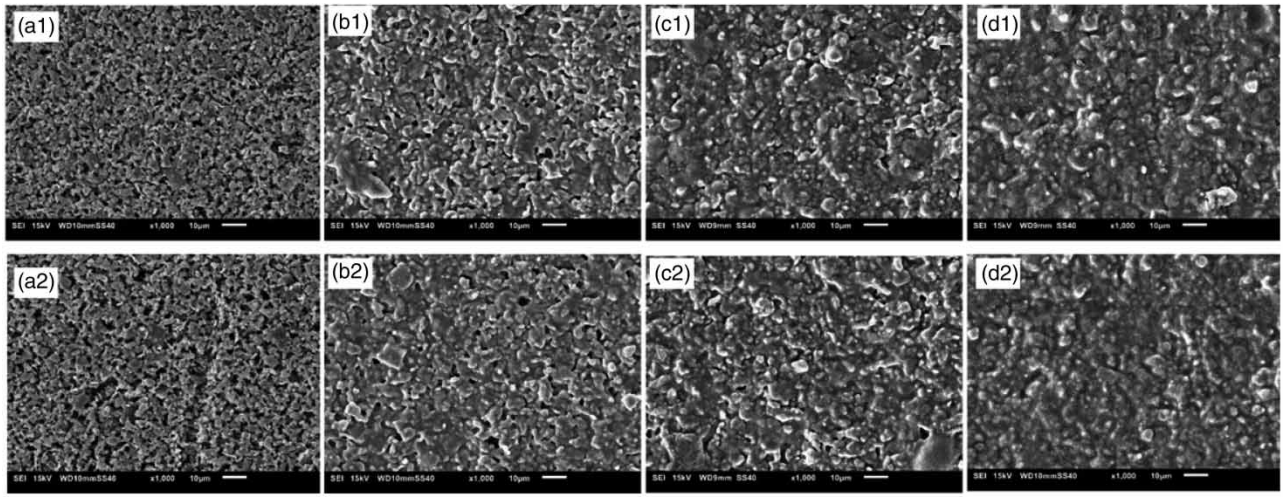

Figure 9 | SEM image of the surface of the metakaolin-based flat sheet ceramic membrane (45 wt.% metakaolin loading). (a1, a2) sintered at 1,200 °C, (b1, b2) sintered at 1,300 °C, (c1, c2) sintered at 1,400 °C, and (d1, d2) sintered at 1,500 °C for 4 h. (a–d) Unmodified membrane, (a1–d1) modified membrane.

structure. The sintered membranes at 1,200, 1,300, 1,400, and 1,500 °C for 4 h showed a regular surface morphology as can be seen in Figure 9. The above observation indicated that the sintering temperature plays an important role in controlling the ceramic membrane porosity and structure. A similar observation was reported in the literature (Ghouil *et al.* 2015; Das *et al.* 2016a, 2016b; Wang *et al.* 2016; Mohtor *et al.* 2017; Mouiya *et al.* 2019).

In addition, it can be observed in Figure 9, that the structural and surface morphology was unchanged after PFAS grafting: this is due to the limited number of hydroxyl groups (OH^-) left on the metakaolin-based ceramic membrane surface after sintering at high temperatures (1,200–1,500 °C) (Fang *et al.* 2012; Hubadillah *et al.* 2018b). It can be concluded that the structure and surface morphology changed gradually with changing composition and sintering temperature (Yang *et al.* 2017; Twibi *et al.* 2021).

3.11. Chemical stability test

Chemical resistance tests of the unmodified kaolin-based ceramic membrane in an acidic (hydrochloric acid, pH = 1) and basic (sodium hydroxide, pH = 14) environment were reported in the previous study (Zewdie *et al.* 2021b). The results showed that the prepared flat ceramic specimen offers good chemical stability in acidic (<3% mass loss in acid solution) and an excellent chemical stability in basic media (<1% mass loss in alkali solution). In this study, the grafted metakaolin-based flat sheet membranes were then immersed into hexane for 120 h at room temperature. After contacting the samples with hexane, the water contact angle of the grafted metakaolin-based ceramic membrane surface was found to be 142.7 ± 0.86° (Figure 10). This shows that the modified membranes demonstrate good chemical stability when treated with a harsh solvent. Besides, insignificant changes in their surface hydrophobicity/wetting properties after being in contact with hexane for 120 h were observed. The stability of the modified membranes in a harsh solvent is due to the strong structure and morphology of the ceramic material. In addition, this confirms that 1H,1H,2H,2H-perfluorodecyltriethoxysilane molecules were covalently attached to the surface as well as inside the porous structure of the metakaolin-based membrane and were stable in hexane (Kujawa *et al.* 2014b). The stability test has shown that the modified metakaolin-based membrane shows good stability in hexane for the PFAS grafting agent.

3.12. Porosity measurements

The porosity of the metakaolin-based flat sheet membranes was determined by the Archimedes method (immersion) using distilled water. In this study, the metakaolin loading and sintering process play an important role in controlling the porosity of the metakaolin-based flat sheet membrane. The experimental data shown in Figure 11 indicate the effect of metakaolin loading and sintering temperature on the porosity of a metakaolin-based flat sheet membrane. According to Figure 11, the porosity of the ceramic membrane decreased with increasing temperature from 1,200 to 1,500 °C, resulting in higher flexural

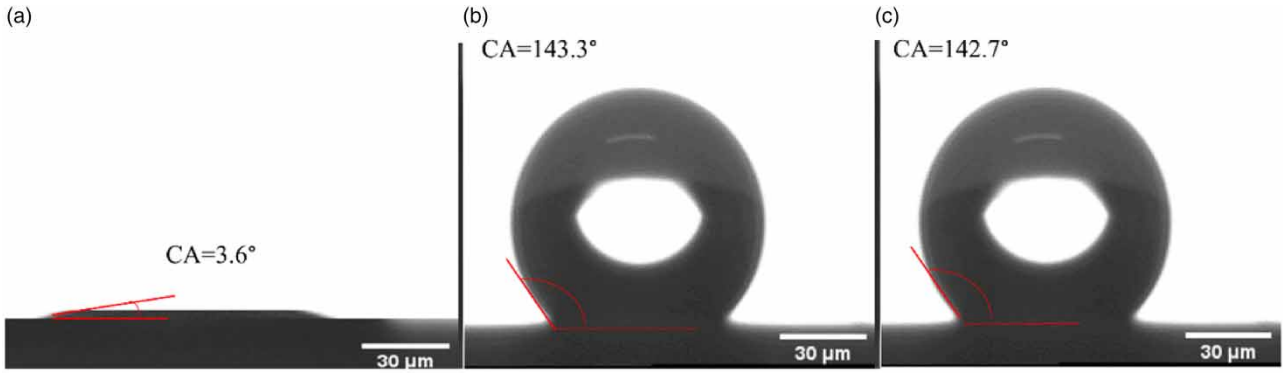

Figure 10 | Chemical stability tests of the metakaolin-based membranes (45 wt.% metakaolin loading, sintered membrane at 1,200 °C) (a) unmodified, (b) modified, and (c) after contact with hexane for 120 h.

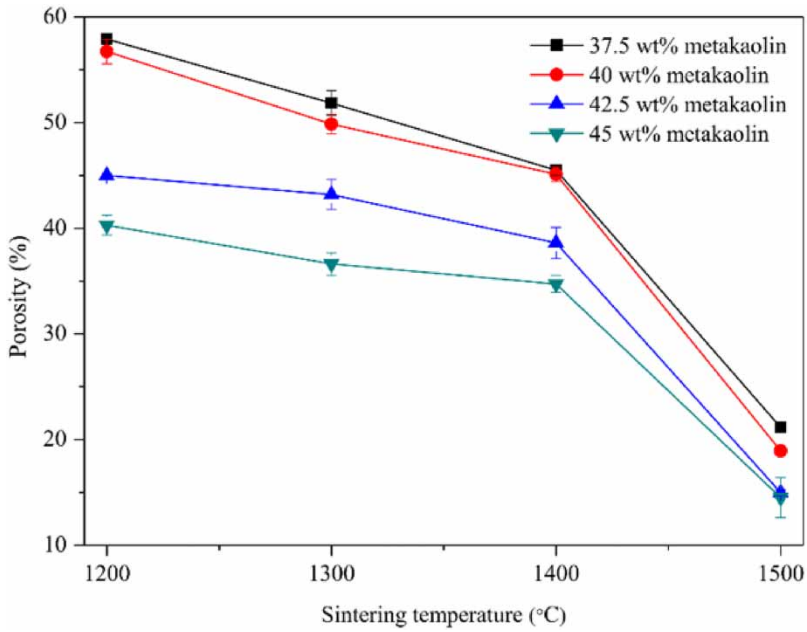

Figure 11 | Variation of average porosity of metakaolin-based flat sheet membrane with different metakaolin contents (37.5–45 wt.%) and sintering temperature (1,200–1,500 °C).

strength (Paiman *et al.* 2015; Mohtor *et al.* 2017; Li *et al.* 2020b). This may be due to the close packing of the particles and the denser texture of the ceramic membrane because, at high temperatures, the particles aggregate and form a cross-linked network structure to attain a further solidified structure.

The values obtained for the porosity of the metakaolin flat sheet membranes (45 wt.% metakaolin loading) slightly decreased from 40.28 ± 0.93% to 36.61 ± 1.07% when sintered at 1,200 and 1,300 °C, respectively. Furthermore, increasing the temperature up to 1,400 and 1,500 °C, the porosity sharply decreases from 34.70 ± 0.8% to 14.50 ± 1.89%, respectively, the latter is due to the significant sintering shrinkage and densification. This decline simultaneously enhances the flexural strength of the membranes. As expected, the membrane porosity decreased when the sintering temperature increased (Guechi *et al.* 2016; Hubadillah *et al.* 2016c, 2019d, 2020; Wang *et al.* 2016; Abdulhameed *et al.* 2017a, 2017b; Mankai *et al.* 2018; Kadiri *et al.* 2020; Li *et al.* 2020b). The micrographs confirm that increasing the sintering temperature decreases the porosity and increases the pore size of the sintered metakaolin-based membrane.

Furthermore, the experimental results indicated that the porosity of the ceramic membrane decreased with increasing metakaolin loading from 37.5 to 45 wt.% (Das *et al.* 2016a, 2016b; Hubadillah *et al.* 2016a, 2016c; Figure 11). Porosity is crucial for a metakaolin-based flat sheet membrane to be used for membrane distillation while providing enough pores for the water

permeation (Fang *et al.* 2012; Hubadillah *et al.* 2016a, 2016c). Hence, controlling the metakaolin loading and sintering temperature is essential for controlling the properties of the metakaolin-based flat sheet membrane (Hubadillah *et al.* 2016a, 2016c). It can be concluded that the porosity of the metakaolin-based flat sheet membranes ranges from 34.70 ± 0.8% to 57.89 ± 0.43%, indicating that the membrane is sufficient for application in the DCMD for water desalination (Khayet 2011; Eykens *et al.* 2016c).

3.13. Mechanical properties

Organic polymer materials such as the polyethersulfone (PES) as a binder and polyethyleneglycol-30 dipolyhydroxystearate (Arlacel P135) as a dispersant in ceramic suspension have to be removed completely from ceramic precursors during the sintering process (Wang *et al.* 2009; Paiman *et al.* 2015), before forming the metakaolin-based flat sheet membrane. Therefore, the metakaolin content in the suspension plays a significant contribution to the flexural strength of the metakaolin-based flat sheet membrane. The increase of the metakaolin content in the ceramic suspension would increase the suspension viscosity. It is a determinantal factor to the flexural strength of metakaolin-based flat sheet membrane. Therefore, to effectively fabricate and produce a low-cost metakaolin-based flat sheet membrane with excellent flexural strength, the higher metakaolin content in the ceramic suspension must be maintained during ceramic suspension preparation (Hubadillah *et al.* 2016a, 2016c). In addition to that, an increase in sintering temperature would enhance the flexural strength of the ceramic membrane. Where, at the higher temperature, the ceramic particles fused and developed larger grains, which gave a higher flexural strength.

The increase in sintering temperature of the metakaolin-based flat sheet membranes (45 wt.% metakaolin loading) raised the flexural strength from 3.4 ± 0.86 MPa to 24.39 ± 1.9 MPa but decreased the porosity of the metakaolin-based flat sheet ceramic membrane from 40.28 ± 0.93% to 14.50 ± 1.89% for temperatures from 1,200 to 1,500 °C, respectively. Findings indicate that the porosity and flexural strength of the metakaolin-based flat sheet membranes can be controlled by varying the metakaolin loading and the sintering temperature.

In general, the flexural strength of ceramic membrane tends to enhance with increasing sintering temperature and decreasing porosity (Sahnoun & Baklouti 2013; Guechi *et al.* 2016; Wang *et al.* 2016; Hubadillah *et al.* 2016c, 2019d, 2020; Abdulhameed *et al.* 2017a, 2017b; Mohamed Bazin *et al.* 2019; Li *et al.* 2020b; Ndjigui *et al.* 2021; Souza *et al.* 2021). Based on the above-observed results, it can be said that a metakaolin-based flat sheet membrane sintered at 1,300, 1,400, and 1,500 °C has a sufficient flexural strength compared to a membrane sintered at 1,200 °C. This is in good agreement with the literature (Feng *et al.* 2004; Essalhi & Khayet 2013; Abdulhameed *et al.* 2017a, 2017b; Mohtor *et al.* 2017). It is seen from Figure 12 that a rapid increase in the flexural strength for 1,500 °C sintered membrane is due to the larger grain growth and densification of the membrane. Thus, it is concluded that the flexural strength of the membranes ranges from 7.3 ± 0.92 to 24.39 ± 1.9 MPa, indicating that the membrane is suitable for application in the DCMD for water desalination (Eykens *et al.* 2016c) and in the filtration process (Sahnoun & Baklouti 2013). Moreover, a metakaolin-based ceramic membrane could be used for a high-strength application at a low cost (Hubadillah *et al.* 2019d).

3.14. Performance of ceramic membrane in DCMD

Previous experimental studies have investigated the effect of flow patterns on permeate flux and salt rejection in desalination by DCMD under countercurrent-flow and concurrent-flow operations. Based on the obtained results, a higher permeate flux was observed in the counter-current flow arrangement. Thus, counter-current flow is preferable to co-current flow (He *et al.* 2011; Hwang *et al.* 2011; Duong *et al.* 2017). Therefore, in this study, a counter-current flow arrangement was applied in all experiments. Moreover, the operational conditions can significantly influence the performance of the membrane distillation process for desalination (Gryta 2012; Zhang *et al.* 2013; Francis *et al.* 2014; Duong *et al.* 2016; Ameen *et al.* 2020). In order to examine the performance of metakaolin-based flat sheet membrane in DCMD the effect of processing time on permeate flux for membranes was investigated. The effect of operating parameters on the permeate flux and salt rejection was assessed. Three parameters at different levels were studied, namely feed temperature in the 50 to 80 °C range, feed flow rate of 30 to 60 L/h, and feed concentration ranging from 0 to 35 g/L.

3.15. Effect of processing time

Based on the characterization results, the metakaolin-based flat sheet membrane sintered at 1,200 °C has inadequate flexural strength (3.4 ± 0.86 MPa). Due to that, the membrane could not withstand the operating conditions (not tolerate higher pressure/feed flow velocity) during the operations, which does not allow for extended process runs (running time: 3 h).

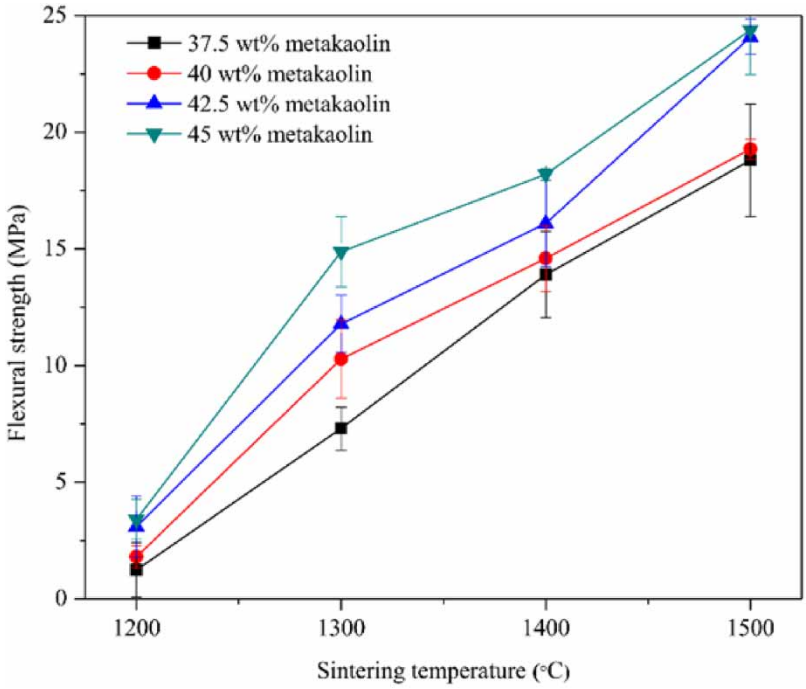

Figure 12 | Effect of metakaolin loading (37.5–45 wt.%) and sintering temperatures (1,200–1,500 °C) on the flexural strength of flat sheet membrane.

Therefore, a preliminary membrane desalination experimental study with a metakaolin-based membrane sintered at 1,200 °C shows a negligible permeate flux (not predict the permeate flux) for the range of feed flow rate tested. Thus, it is not suitable for membrane distillation (Eykens *et al.* 2016c). Figure 13 shows the change in the permeate flux as a function of process time

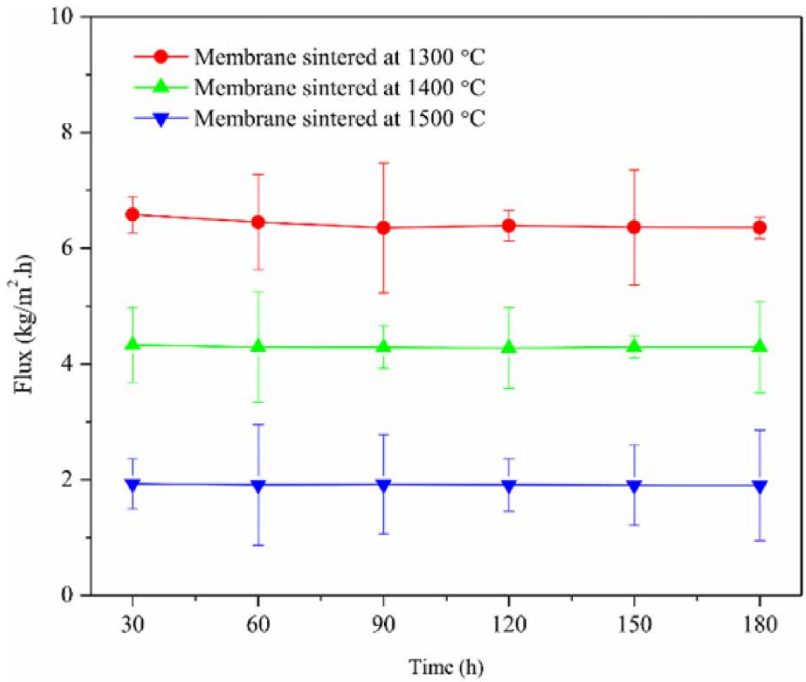

Figure 13 | Variation of permeate flux with time for membranes sintered at different temperatures (1,300, 1,400, and 1,500 °C). Experimental conditions: feed solution: 35 g/L NaCl, permeate: DI water, feed inlet temperature: 80 °C, coolant inlet temperature: 20 °C, volumetric flow rate of feed and permeate inlet: 60 L/h, flow pattern: counter-current, running time: 3 h.

for metakaolin-based membranes sintered at different temperatures (1,300, 1,400, and 1,500 °C). The results demonstrate that the behavior of the permeate flux as a function of process time consists of two distinct stages: In the first stage, the permeate flux declined. In the second stage of the process, a constant permeate flux was observed. Permeate flux decreased with process time in all experimental runs for all membranes. A slight decline in the permeate flux was observed during the first 60 min for all membranes. The permeate flux remained constant after 60 min for time on stream of 180 min. The obtained results showed that the metakaolin-based flat sheet membrane sintered at 1,300 °C has the highest water permeation of 6.58 ± 0.3 kg/m^2 h, followed by the membranes sintered at 1,400 and 1,500 °C with a water permeation of 4.33 ± 0.65 and 1.93 ± 0.43 kg/m^2 h, respectively. This is due to the slightly higher porosity of the metakaolin-based membrane sintered at 1,300 °C (about 36.61 ± 1.07%) compared to membranes sintered at 1,400 °C (about 34.70 ± 0.8%) and 1,500 °C (about 14.50 ± 1.89%). The metakaolin-based flat sheet membranes showed a comparable performance (permeate flux) results reported elsewhere (Kujawa *et al.* 2014a; Zhang *et al.* 2014; Wang *et al.* 2016; Hubadillah *et al.* 2019e).

3.16. Effect of feed temperature

Feed temperature is a key operational parameter for DCMD. The permeate flux and salt rejection of metakaolin-based flat sheet membrane for artificial saline water during 3 h running time at different feed temperatures in counter-current flow operation are presented in Figure 14. Typically, the temperature at the feed stream is adjustable and the temperature at the coolant inlet stream is fixed to study the effect of temperature on permeate flux and salt rejection. The feed temperature was investigated in the range of 50 to 80 °C at 10 °C intervals with a feed solution of 35 g/L; the feed inlet flow rate, coolant inlet flow rate, and temperature were maintained at 60 L/h, 60 L/h, and 20 ± 0.5 °C, respectively.

At feed inlet temperatures 50, 60, 70, and 80 °C, the permeate flux increases were 2.58 ± 0.21, 3.17 ± 0.09, then 5.67 ± 0.11, and 6.58 ± 0.3. These results reflected the increase of the permeate flux, when the feed inlet temperature increased from 50 to 80 °C for a fixed feed inlet solution of 35 g/L, and permeate inlet temperature of 20 ± 0.5 °C. The vapor pressure of a liquid increases exponentially with feed inlet temperature, as described in the Antoine equation. Therefore, at high feed inlet temperatures, the permeate flux increased exponentially. The obtained results are in good agreement with the previously reported results (Fang *et al.* 2012; Singh & Sirkar 2012; Kujawa *et al.* 2014a; Lee *et al.* 2015; Shim *et al.* 2015; Khalifa *et al.* 2017; Luo & Lior 2017; Ameen *et al.* 2020; Twibi *et al.* 2021).

Interestingly, the salt rejections remained almost constant as the feed inlet temperature increased from 50 °C (salt rejection: 95.17 ± 0.2%) to 80 °C (salt rejection: 95.0 ± 0.17%). The high salt rejection (>95%), as shown in Figure 14, indicates the good desalination performance in the DCMD process.

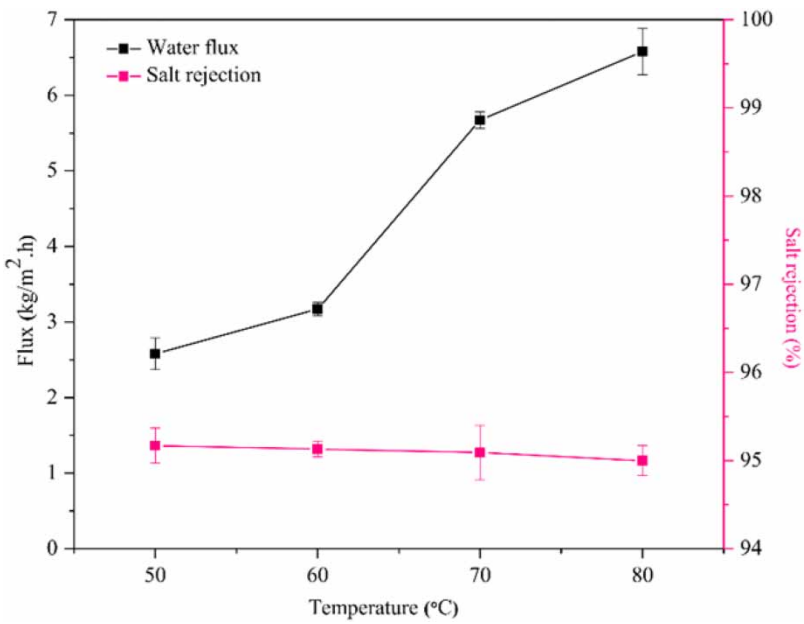

Figure 14 | Effect of feed temperature on permeate flux and salt rejection. Experimental conditions: feed solution: 35 g/L NaCl, permeate: DI water, coolant inlet temperature: 20 °C, volumetric flow rate of feed and permeate inlet: 60 L/h, flow pattern: counter-current, running time: 3 h.

3.17. Effect of feed flow rate

The influence of feed inlet flow rate on the permeate flux and salt rejection in the DCMD process in counter-current flow is illustrated in Figure 15. The increase in feed inlet flow rate in the DCMD process ranging from 30 to 60 L/h, leads to an increase in the permeate flux from 2.03 ± 0.14 to 6.58 ± 0.3 kg/m^2 h for a feed concentration of 35 g/L, at a feed inlet temperature of 80 °C and a constant coolant inlet flow rate and temperature of 60 L/h and 20 ± 0.5 °C, respectively. As displayed in Figure 15, the permeate flux increased linearly with increasing feed flow rate. In most previous studies, the permeate fluxes increased with the feed flow rate (Shirazi *et al.* 2014; Shim *et al.* 2015). Generally, a higher feed flow rate leads to higher turbulence, which results in the better mixing of the feed solution, which in turn enhanced the mass and heat transfer coefficient (Qusay *et al.* 2017; Chen *et al.* 2020). This is due to the reduction in the temperature and concentration polarization boundary layer thickness. Thus, the temperature difference across the membrane sides increased and resulted in an improved permeate flux (Qusay *et al.* 2017).

Furthermore, it can be seen from Figure 15 that the salt rejection is slightly lower at a higher feed flow rate. This is due to the lower residence time inside the membrane distillation module with high feed flow rates and therefore enhanced heat loss by conduction and poor heat recovery (Guillén-Burrieza *et al.* 2015; Subrahmanya *et al.* 2021).

3.18. Effect of feed concentration

The experiments were carried out at various feed concentrations (i.e., 5, 15, 25, and 35 g/L NaCl) in counter-current flow keeping the feed inlet temperature, coolant inlet temperature, and feed and coolant flow rate at constant values of 80 °C, 20 °C, and 60 L/h, respectively. Figure 16 shows the effect of the feed concentration on the permeate flux and salt rejection at constant feed flow rates.

The results demonstrated that the permeate flux slightly decreased with increasing the feed salt concentration from 5 to 35 g/L. Many studies reported that permeate flux in the DCMD process decrease with increasing feed salt concentration because the water vapor pressure decreases at higher feed salt concentration based on Raoult's law (Fang *et al.* 2012; Kujawa *et al.* 2014a, 2016; Hubadillah *et al.* 2018b; Twibi *et al.* 2021). This is because more salt molecules are deposited and accumulated on the membrane surface at the feed side, formation of fouling/scaling layer on the membrane surface, an increase of resistance in transfer, and induced wetting of the membrane on the feed side which ultimately leading in a vapor pressure reduction. Moreover, it causes a decrease of the driving force across the membrane and an increase of salt

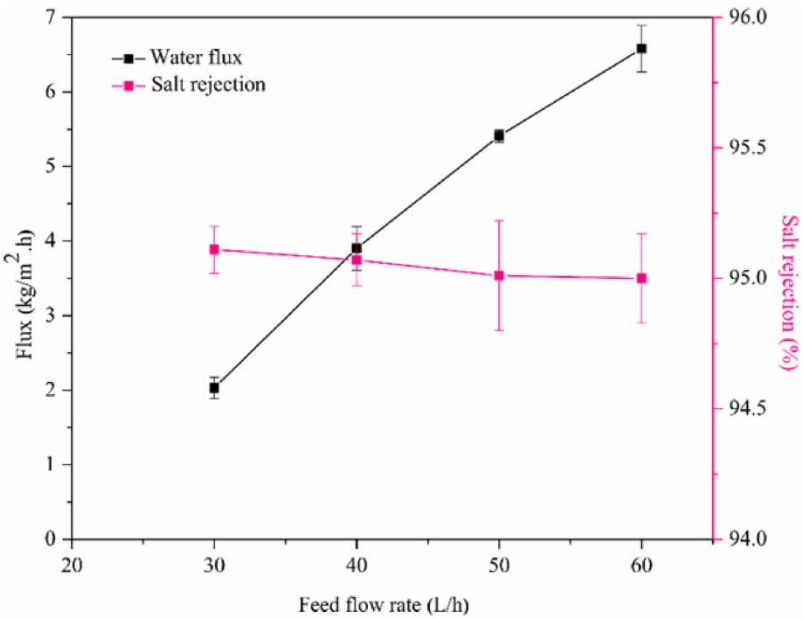

Figure 15 | Effect of feed flow rate on permeate flux and salt rejection. Experimental conditions: feed solution: 35 g/L NaCl, permeate: DI water, feed inlet temperature: 80 °C, coolant inlet temperature: 20 °C, volumetric flow rate of permeate inlet: 60 L/h, flow pattern: counter-current, running time: 3 h.

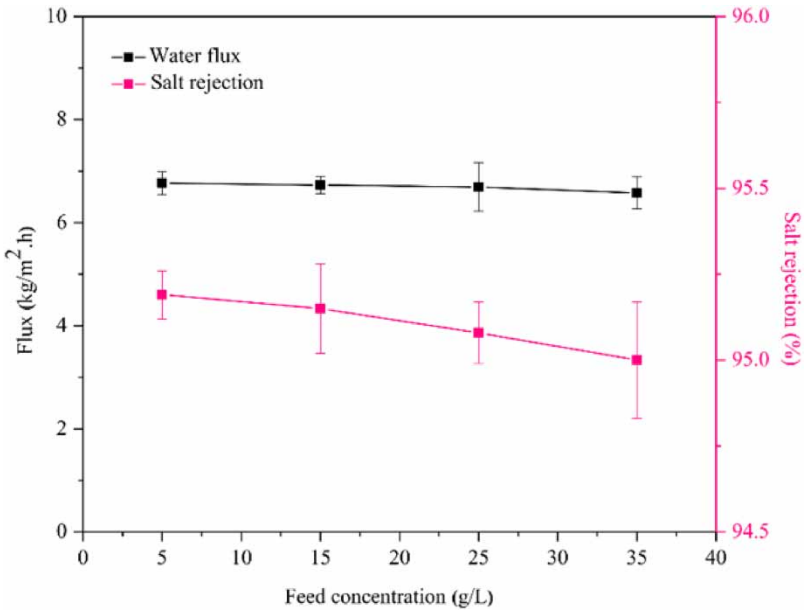

Figure 16 | Effect of feed concentration on permeate flux and salt rejection. Experimental conditions: permeate: DI water, feed inlet temperature: 80 °C, coolant inlet temperature: 20 °C, volumetric flow rate of feed and permeate inlet: 60 L/h, flow pattern: counter-current, running time: 3 h.

concentration of permeate flux. Thus, this study and others (Qusay *et al.* 2017; Ameen *et al.* 2020) all confirmed that salt rejection decreases with increasing salt concentration.

Table 2 lists the comparison between several studies reporting on ceramic membrane properties (hydrophobicity) and performances (permeate flux and salt rejection) along with study results. The permeate flux and salt rejection obtained in this study were low (permeate flux: 1.9–6.58 kg/m^2 h, salt rejection: >95%) compared to previous studies on hollow fiber and tubular membrane module for a feed temperature of 80 °C (see Table 2). The obtained results for the prepared metakaolin-based flat sheet membrane sintered at 1,300 °C (45 wt.% metakaolin loading) can be explained by the lower porosity (36.61 $\pm$ 1.07%) and flexural strength (14.88 $\pm$ 1.5 MPa). Despite the relatively low performance, there is no study yet on the performance of metakaolin-based flat sheet membrane in terms of water permeate flux and salt rejection using DCMD to directly compare with our findings. This work shows that the properties of metakaolin-based flat sheet membranes can be further fine-tuned to obtain a better membrane performance. Therefore, metakaolin-based flat sheet membrane fabrication needs further investigation under different membrane preparation parameters (metakaolin loading, sintering temperature, the concentration of the additives, and mixing practice) to obtain desirable separation performances (permeate flux and salt rejection) as well as membrane properties (porosity and flexural strength). Nevertheless, considering the abundant availability and further refined the preparation methods. It will be an attractive alternative for seawater desalination in the membrane distillation process and can achieve comparable membrane performance with hollow fiber and tubular membrane modules.

4. CONCLUSION

This study was concerned with the development and characterization of hydrophobic metakaolin-based flat sheet ceramic membranes for water desalination by DCMD. Based on the findings or outcomes of the present studies, the following conclusions can be drawn:

Based on the findings, the metakaolin loading of 45 wt.% and the sintering temperature of 1,300 °C could be selected as the best parameters in preparing the metakaolin flat sheet membrane and provided desirable membrane performance in terms of porosity, flexural strength, hydrophobicity, water permeate flux, and salt rejection.

It was noted that the most significant operating variable affecting the performance of the DCMD process was the feed temperature. To a lower extent, the feed flow rate and concentration had a clear effect on the permeate flux. The permeate flux

Table 2 | Comparison of the permeate flux and salt rejection at 80 °C obtained in this study with the literature values for the DCMD process

No	Membrane materials	Membrane module type	Modifying agent (PFAS)	Application	Contact angle (°)	Porosity (%)	Permeate flux ($kg/m^2 \cdot h$)	Salt rejection (%)	Reference
1	Titania	Tubular	1H,1H,2H,2H-perfluorooctyltriethoxysilane	Desalination (NaCl)	135–145	–	0.9–3.0	>99	Kujawa *et al.* (2014a)
2	Silicon nitride	Hollow fiber	1H,1H,2H,2H-perfluorooctyltriethoxysilane	Desalination (NaCl)	136	50	9.2	>99	Zhang *et al.* (2014)
3	β-Sialon	Hollow fiber	1H,1H,2H,2H-perfluorooctyltriethoxysilane	Desalination (NaCl)	125	48	12.2	>99	Wang *et al.* (2016)
4	Green Silica	Hollow fiber	1H,1H,2H,2H-perfluorodecyltriethoxysilane	Desalination (NaCl)	157–161	35.86–54.12	38.2–52.4	99.9	Hubadilla *et al.* (2018b)
5	Metakaolin	Hollow fiber	1H,1H,2H,2H-perfluorodecyltriethoxysilane	Deionized water	120	–	5.3–16.5	–	Hubadillah *et al.* (2019e)
6	Mullite	Hollow fiber	1H,1H,2H,2H-perfluorodecyltriethoxysilane	Desalination (NaCl)	139	43	30.55	99.99	Twibi *et al.* (2021)
7	Metakaolin	Flat sheet	1H,1H,2H,2H-perfluorooctyltriethoxysilane	Desalination (NaCl)	113.2–143.3	14.88–36.61	1.9–6.58	>95	This study

reached 6.58 ± 0.3 kg/m^2 h and salt rejection was as high as 95%, the feed inlet temperature was 80 °C and the feed inlet flow rate and concentration were 60 L/h and 35 g/L NaCl, respectively.

The flux and salt rejections reported in this work (flat sheet membrane module) are low compared to those reported in the literature (hollow fiber and tubular membrane modules) (see Table 2). This can be attributed to the low membrane porosity (36.61 ± 1.07%). Thus, this study could provide new insights on the utilization of metakaolin-based flat sheet membranes in the field of the advanced separation process. Nevertheless, further optimization of membrane porosity, mechanical, and surface properties is required to maximize the permeate flux and salt rejection.

ACKNOWLEDGEMENTS

The author would like to thank and appreciate the Ethiopian government/Ministry of Higher Education and the German government for their financial support and special thanks to the KU Leuven and the Bahir Dar University, for providing the necessary facilities for this research.

DATA AVAILABILITY STATEMENT

All relevant data are included in the paper or its Supplementary Information.

REFERENCES

Abd Aziz, M. H., Othman, M. H. D., Hashim, N. A., Adam, M. R. & Mustafa, A. 2019 Fabrication and characterization of mullite ceramic hollow fiber membrane from natural occurring ball clay. *Applied Clay Science* **177**, 51–62.

Abdelrazeq, H., Khraisheh, M., Al Momani, F., McLeskey Jr, J. T., Hassan, M. K., Gad-el-Hak, M. & Tafreshi, H. V. 2020 Performance of electrospun polystyrene membranes in synthetic produced industrial water using direct-contact membrane distillation. *Desalination* **493**, 114663.

Abdulhameed, M. A., Othman, M. H. D., Ismail, A. F., Matsuura, T., Harun, Z., Rahman, M. A., Puteh, M. H. & Jaafar, J. 2017a Preparation and characterisation of inexpensive porous kaolin hollow fibre as ceramic membrane supports for gas separation application. *Journal of the Australian Ceramic Society* **53** (2), 645–655.

Abdulhameed, M. A., Othman, M. H. D., Joda, H. N. A. A., Ismail, A. F., Matsuura, T., Harun, Z., Puteh, M. H. & Jaafar, J. 2017b Fabrication and characterization of affordable hydrophobic ceramic hollow fibre membrane for contacting processes. *Journal of Advanced Ceramics* **6** (4), 330–340.

Abu-Zeid, M. A. E. R., Zhang, Y., Dong, H., Zhang, L., Chen, H. L. & Hou, L. 2015 A comprehensive review of vacuum membrane distillation technique. *Desalination* **356**, 1–14.

Aliyu, U. M., Rathilal, S. & Isa, Y. M. 2018 Membrane desalination technologies in water treatment: a review. *Water Practice and Technology* **13** (4), 738–752.

Alkhudhiri, A. & Hilal, N. 2018 *Membrane Distillation-Principles, Applications, Configurations, Design, and Implementation, Emerging Technologies for Sustainable Desalination Handbook*. Butterworth-Heinemann, Elsevier Inc, pp. 55–106.

Al-Naib, U. M. B. 2018 Introductory chapter: a brief introduction to porous ceramic. *Recent Advances in Porous Ceramics* **10**, 1–10.

Ameen, N. A. M., Ibrahim, S. S., Alsalhy, Q. F. & Figoli, A. 2020 Highly saline water desalination using direct contact membrane distillation (DCMD): experimental and simulation study. *Water* **12** (6), 1575.

Aragaw, T. A. & Angerasa, F. T. 2020 Synthesis and characterization of Ethiopian kaolin for the removal of basic yellow (BY 28) dye from aqueous solution as a potential adsorbent. *Heliyon* **6** (9), e04975.

Arumugham, T., Kaleekkal, N. J., Gopal, S., Nambikkattu, J., Rambabu, K., Aboulella, A. M., Wickramasinghe, S. R. & Banat, F. 2021 Recent developments in porous ceramic membranes for wastewater treatment and desalination: a review. *Journal of Environmental Management* **293**, 112925.

Ashoor, B. B., Giwa, A. & Hasan, S. W. 2018 *Full-Scale Membrane Distillation Systems and Performance Improvement Through Modeling: A Review, Current Trends and Future Developments on (Bio-) Membranes: Membrane Desalination Systems: The Next Generation*. Elsevier Inc., Masdar city, Abu Dhabi, pp. 105–140.

Bandar, K. B., Alsubei, M. D., Aljlil, S. A., Darwish, N. B. & Hilal, N. 2021 Membrane distillation process application using a novel ceramic membrane for Brackish water desalination. *Desalination* **500**, 114906.

Baten, R. & Stummeyer, K. 2013 How sustainable can desalination be? *Desalination and Water Treatment* **51** (1–3), 44–52.

Belessiotis, V., Kalogirou, S. & Delyannis, E. 2016 Chapter four – Membrane distillation. *Thermal Solar Desalination: Methods and Systems* **201**, 191–251.

Bikel, M., Pünt, I. G. M., Lammertink, R. G. & Wessling, M. 2010 Shrinkage effects during polymer phase separation on microfabricated molds. *Journal of Membrane Science* **347** (1-2), 141–149.

Bonyadi, S., Chung, T. S. & Krantz, W. B. 2007 Investigation of corrugation phenomenon in the inner contour of hollow fibers during the non-solvent induced phase-separation process. *Journal of Membrane Science* **299** (1–2), 200–210.

Boussemghoune, M., Chikhi, M., Ozay, Y., Guler, P., Ozbey Unal, B. & Dizge, N. 2020 The investigation of organic binder effect on morphological structure of ceramic membrane support. *Symmetry* **12** (5), 770.

Brusseau, M. L., Ramirez-Andreotta, M., Pepper, I. L. & Maximillian, J. 2019 Environmental impacts on human health and well-being. *Environmental and Pollution Science*, 3rd edn. 477–499.

Chen, G., Qi, H., Xing, W. & Xu, N. 2008 Direct preparation of macroporous mullite supports for membranes by in situ reaction sintering. *Journal of Membrane Science* **318** (1-2), 38–44.

Chen, L., Xu, P. & Wang, H. 2020 Interplay of the factors affecting water flux and salt rejection in membrane distillation: a state-of-the-art critical review. *Water (Switzerland)* **12** (10), 2841.

Cheng, Y., Xing, J., Bu, C., Zhang, J., Piao, G., Huang, Y. & Wang, X. 2019 Dehydroxylation and structural distortion of kaolinite as a high-temperature sorbent in the furnace. *Minerals* **9** (10), 587.

dan Sinteran, F. 2017 A fabrication of a low-cost zeolite based ceramic membrane via phase inversion and sintering technique. *Malaysian Journal of Analytical Sciences* **21** (2), 391–401.

Das, B., Chakrabarty, B. & Barkakati, P. 2016a Preparation and characterization of novel ceramic membranes for micro-filtration applications. *Ceramics International* **42** (13), 14326–14333.

Das, R., Sondhi, K., Majumdar, S. & Sarkar, S. 2016b Development of hydrophobic clay–alumina based capillary membrane for desalination of brine by membrane distillation. *Journal of Asian Ceramic Societies* **4** (3), 243–251.

Dinakar, P., Sahoo, P. K. & Sriram, G. 2013 Effect of metakaolin content on the properties of high strength concrete. *International Journal of Concrete Structures and Materials* **7** (3), 215–223.

Djobo, J. Y., Tchadjié, L. N., Tchakoute, H. K., Kenne, B. B. D., Elimbi, A. & Njopwouo, D. 2014 Synthesis of geopolymer composites from a mixture of volcanic scoria and metakaolin. *Journal of Asian Ceramic Societies* **2** (4), 387–398.

Dong, S., Yun, Y., Wang, M., Li, C., Fu, H., Li, X., Yang, W. & Liu, G. 2020 Superhydrophobic alumina hollow ceramic membrane modified by TiO_2 nanorod array for vacuum membrane distillation. *Journal of the Taiwan Institute of Chemical Engineers* **117**, 56–62.

Douiri, H., Louati, S., Baklouti, S., Arous, M. & Fakhfakh, Z. 2017 Structural and dielectric comparative studies of geopolymers prepared with metakaolin and Tunisian natural clay. *Applied Clay Science* **139**, 40–44.

Duong, H. C., Cooper, P., Nelemans, B., Cath, T. Y. & Nghiem, L. D. 2016 Evaluating energy consumption of membrane distillation for seawater desalination using a pilot air gap system. *Separation and Purification Technology* **166**, 55–62.

Duong, H. C., Xia, L., Ma, Z., Cooper, P., Ela, W. & Nghiem, L. D. 2017 Assessing the performance of solar thermal driven membrane distillation for seawater desalination by computer simulation. *Journal of Membrane Science* **542**, 133–142.

Elgamouz, A., Tijani, N., Shehadi, I., Hasan, K. & Kawam, M. A. F. 2019 Characterization of the firing behaviour of an illite-kaolinite clay mineral and its potential use as membrane support. *Heliyon* **5** (8), e02281.

Espiritu, R., Mamlouk, M. & Scott, K. 2016 Study on the effect of the degree of grafting on the performance of polyethylene-based anion exchange membrane for fuel cell application. *International Journal of Hydrogen Energy* **41** (2), 1120–1133.

Essalhi, M. & Khayet, M. 2013 Self-sustained webs of polyvinylidene fluoride electrospun nanofibers at different electrospinning times: 1. Desalination by direct contact membrane distillation. *Journal of Membrane Science* **433**, 167–179.

Eykens, L., Reyns, T., De Sitter, K., Dotremont, C., Pinoy, L. & Van der Bruggen, B. 2016a How to select a membrane distillation configuration? Process conditions and membrane influence unraveled. *Desalination* **399**, 105–115.

Eykens, L., Hitsov, I., De Sitter, K., Dotremont, C., Pinoy, L., Nopens, I. & Van der Bruggen, B. 2016b Influence of membrane thickness and process conditions on direct contact membrane distillation at different salinities. *Journal of Membrane Science* **498**, 353–364.

Eykens, L., De Sitter, K., Dotremont, C., Pinoy, L. & Van der Bruggen, B. 2016c How to optimize the membrane properties for membrane distillation: a review. *Industrial & Engineering Chemistry Research* **55** (35), 9333–9343.

Fang, H., Gao, J. F., Wang, H. T. & Chen, C. S. 2012 Hydrophobic porous alumina hollow fiber for water desalination via membrane distillation process. *Journal of Membrane Science* **403**, 41–46.

Feng, C., Shi, B., Li, G. & Wu, Y. 2004 Preliminary research on microporous membrane from F2.4 for membrane distillation. *Separation and Purification Technology* **39** (3), 221–228.

Feria-Díaz, J. J., López-Méndez, M. C., Rodríguez-Miranda, J. P., Sandoval-Herazo, L. C. & Correa-Mahecha, F. 2021 Commercial thermal technologies for desalination of water from renewable energies: a state of the art review. *Processes* **9** (2), 262.

Francis, L., Ghaffour, N., Alsaadi, A. S., Nunes, S. P. & Amy, G. L. 2014 Performance evaluation of the DCMD desalination process under bench scale and large scale module operating conditions. *Journal of Membrane Science* **455**, 103–112.

Ghaffour, N., Soukane, S., Lee, J. G., Kim, Y. & Alpatova, A. 2019 Membrane distillation hybrids for water production and energy efficiency enhancement: a critical review. *Applied Energy* **254**, 113698.

Ghouil, B., Harabi, A., Bouzerara, F., Boudaira, B., Guechi, A., Demir, M. M. & Figoli, A. 2015 Development and characterization of tubular composite ceramic membranes using natural alumino-silicates for microfiltration applications. *Materials Characterization* **103**, 18–27.

Gomez, M., Perdiguero, J. & Sanz, A. 2019 Socioeconomic factors affecting water access in rural areas of low and middle income countries. *Water* **11** (2), 202.

Green, D. J., Guillon, O. & Rödel, J. 2008 Constrained sintering: a delicate balance of scales. *Journal of the European Ceramic Society* **28** (7), 1451–1466.

Gryta, M. 2012 Effectiveness of water desalination by membrane distillation process. *Membranes* **2** (3), 415–429.

Gude, V. G. 2018 *Energy Storage for Desalination, Renewable Energy Powered Desalination Handbook: Application and Thermodynamics*. Butterworth-Heinemann, Elsevier Inc., pp. 377–414.

Guechi, A., Harabi, A., Condoum, S., Zenikheri, F., Boudaira, B., Bouzerara, F. & Foughali, L. 2016 Elaboration and characterization of tubular supports for membranes filtration. *Desalination and Water Treatment* **57** (12), 5246–5252.

Gugliuzza, A. & Basile, A. 2013 *Membrane Contactors: Fundamentals, Membrane Materials and Key Operations, Handbook of Membrane Reactors*, Vol. 2. Woodhead Publishing Limited, Cambridge, UK, pp. 54–106.

Guillén-Burrieza, E., Alarcón-Padilla, D. C., Palenzuela, P. & Zaragoza, G. 2015 Techno-economic assessment of a pilot-scale plant for solar desalination based on existing plate and frame MD technology. *Desalination* **374**, 70–80.

Hakami, M. W., Alkhudhiri, A., Al-Batty, S., Zacharof, M. P., Maddy, J. & Hilal, N. 2020 Ceramic microfiltration membranes in wastewater treatment: filtration behavior, fouling and prevention. *Membranes* **10** (9), 248.

Hara, E., Yokozeki, T., Hatta, H., Iwahori, Y. & Ishikawa, T. 2014 Comparison of out-of-plane tensile moduli of CFRP laminates obtained by 3-point bending and direct loading tests. *Composites Part A: Applied Science and Manufacturing* **67**, 77–85.

Harabi, A., Zenikheri, F., Boudaira, B., Bouzerara, F., Guechi, A. & Foughali, L. 2014 A new and economic approach to fabricate resistant porous membrane supports using kaolin and $CaCO_3$. *Journal of the European Ceramic Society* **34** (5), 1329–1340.

He, K., Hwang, H. J., Woo, M. W. & Moon, I. S. 2011 Production of drinking water from saline water by direct contact membrane distillation (DCMD). *Journal of Industrial and Engineering Chemistry* **17** (1), 41–48.

Hernández-Aguirre, O. A., Nunez-Pineda, A., Tapia-Tapia, M. & Gomez Espinosa, R. M. 2016 Surface modification of polypropylene membrane using biopolymers with potential applications for metal ion removal. *Journal of Chemistry* **2016**, 2742013.

Hubadillah, S. K., Harun, Z., Othman, M. H. D., Ismail, A. F. & Gani, P. 2016a Effect of kaolin particle size and loading on the characteristics of kaolin ceramic support prepared via phase inversion technique. *Journal of Asian Ceramic Societies* **4** (2), 164–177.

Hubadillah, S. K., Harun, Z., Othman, M. H. D., Ismail, A. F., Salleh, W. N. W., Basri, H., Yunos, M. Z. & Gani, P. 2016b Preparation and characterization of low cost porous ceramic membrane support from kaolin using phase inversion/sintering technique for gas separation: effect of kaolin content and non-solvent coagulant bath. *Chemical Engineering Research and Design* **112**, 24–35.

Hubadillah, S. K., Othman, M. H. D., Harun, Z., Ismail, A. F., Iwamoto, Y., Honda, S. & Sokri, M. N. M. 2016c Effect of fabrication parameters on physical properties of metakaolin-based ceramic hollow fibre membrane (CHFM). *Ceramics International* **42** (14), 15547–15558.

Hubadillah, S. K., Othman, M. H. D., Matsuura, T., Ismail, A. F., Rahman, M. A., Harun, Z., Jaafar, J. & Nomura, M. 2018a Fabrications and applications of low cost ceramic membrane from kaolin: a comprehensive review. *Ceramics International* **44** (5), 4538–4560.

Hubadillah, S. K., Othman, M. H. D., Matsuura, T., Rahman, M. A., Jaafar, J., Ismail, A. F. & Amin, S. Z. M. 2018b Green silica-based ceramic hollow fiber membrane for seawater desalination via direct contact membrane distillation. *Separation and Purification Technology* **205**, 22–31.

Hubadillah, S. K., Kumar, P., Othman, M. H. D., Ismail, A. F., Rahman, M. A. & Jaafar, J. 2018c A low cost, superhydrophobic and superoleophilic hybrid kaolin-based hollow fibre membrane (KHFM) for efficient adsorption–separation of oil removal from water. *RSC Advances* **8** (6), 2986–2995.

Hubadillah, S. K., Tai, Z. S., Othman, M. H. D., Harun, Z., Jamalludin, M. R., Rahman, M. A., Jaafar, J. & Ismail, A. F. 2019a Hydrophobic ceramic membrane for membrane distillation: a mini review on preparation, characterization, and applications. *Separation and Purification Technology* **217**, 71–84.

Hubadillah, S. K., Othman, M. H. D., Ismail, A. F., Rahman, M. A. & Jaafar, J. 2019b A low cost hydrophobic kaolin hollow fiber membrane (h-KHFM) for arsenic removal from aqueous solution via direct contact membrane distillation. *Separation and Purification Technology* **214**, 31–39.

Hubadillah, S. K., Othman, M. H. D., Kadir, S. H. S. A., Jamalludin, M. R., Harun, Z., Abd Aziz, M. H., Rahman, M. A., Jaafar, J., Nomura, M., Honda, S., Iwamoto, Y. & Fansuri, H. 2019c Removal of As (III) and As (V) from water using green, silica-based ceramic hollow fibre membranes via direct contact membrane distillation. *RSC Advances* **9** (6), 3367–3376.

Hubadillah, S. K., Othman, M. H. D., Harun, Z., Jamalludin, M. R., Zahar, M. I. I. M., Ismail, A. F., Rahman, M. A. & Jaafar, J. 2019d High strength and antifouling metakaolin-based ceramic membrane for juice clarification. *Journal of the Australian Ceramic Society* **55** (2), 529–540.

Hubadillah, S. K., Othman, M. H. D., Ismail, A. F., Rahman, M. A. & Jaafar, J. 2019e Morphological study of hydrophobic metakaolin hollow fibre membrane for membrane distillation application. *Malaysian Journal of Fundamental and Applied Sciences* **15** (3), 478–482.

Hubadillah, S. K., Othman, M. H. D., Rahman, M. A., Ismail, A. F. & Jaafar, J. 2020 Preparation and characterization of inexpensive kaolin hollow fibre membrane (KHFM) prepared using phase inversion/sintering technique for the efficient separation of real oily wastewater. *Arabian Journal of Chemistry* **13** (1), 2349–2367.

Hubadillah, S. K., Hami, N., Salleh, N. A., Jamalludin, M. R., Harun, Z., Othman, M. H. D. & Hairom, N. H. H. 2021 Effect of kaolin particle size towards preparation of kaolin ceramic membrane. *Emerging Advances in Integrated Technology* **2** (1), 18–24.

Hussain, A., Janson, A., Matar, J. M. & Adham, S. 2021 Membrane distillation: recent technological developments and advancements in membrane materials. *Emergent Materials* **4**, 1–21.

Hwang, H. J., He, K., Gray, S., Zhang, J. & Moon, I. S. 2011 Direct contact membrane distillation (DCMD): experimental study on the commercial PTFE membrane and modeling. *Journal of Membrane Science* **371** (1–2), 90–98.

Izadifar, M., Thissen, P., Steudel, A., Kleeberg, R., Kaufhold, S., Kaltenbach, J., Schuhmann, R., Dehn, F. & Emmerich, K. 2020 Comprehensive examination of dehydroxylation of kaolinite, disordered kaolinite, and dickite: experimental studies and Density Functional Theory. *Clays and Clay Minerals* **68** (4), 319–333.

Ji, S., Liu, Z., Wang, G., Liu, Y. & Jing, Y. 2020 Effects of sintering temperature and particle size on permeability of functionally gradient composite porous materials prepared by hanging slurry process. *SN Applied Sciences* **2** (12), 1–20.

Jiang, F., Zhang, L., Jiang, Z., Li, C., Cang, D., Liu, X., Xuan, Y. & Ding, Y. 2019 Diatomite-based porous ceramics with high apparent porosity: pore structure modification using calcium carbonate. *Ceramics International* **45** (5), 6085–6092.

Kadiri, C., Harabi, A., Bouzerara, F., Foughali, L., Brihi, N., Hallour, S. & Boudaira, B. 2020 Preparation and properties of tubular macroporous ceramic membrane supports based on natural quartz sand and dolomite. *Journal of the Australian Ceramic Society* **56** (2), 379–387.

Khalifa, A., Ahmad, H., Antar, M., Laoui, T. & Khayet, M. 2017 Experimental and theoretical investigations on water desalination using direct contact membrane distillation. *Desalination* **404**, 22–34.

Khan, M. I., Khan, H. U., Azizli, K., Sufian, S., Man, Z., Siyal, A. A., Muhammad, N. & ur Rehman, M. F. 2017 The pyrolysis kinetics of the conversion of Malaysian kaolin to metakaolin. *Applied Clay Science* **146**, 152–161.

Khatib, J. M., Baalbaki, O. & ElKordi, A. A. 2018 Metakaolin, waste and supplementary cementitious materials in concrete: characterisation. *Properties and Applications* **15**, 493–511.

Khayet, M. 2011 Membranes and theoretical modeling of membrane distillation: a review. *Advances in Colloid and Interface Science* **164** (1–2), 56–88.

Khemakhem, S. & Amar, R. B. 2011 Modification of Tunisian clay membrane surface by silane grafting: application for desalination with air gap membrane distillation process. *Colloids and Surfaces A: Physicochemical and Engineering Aspects* **387** (1–3), 79–85.

Khemakhem, M., Khemakhem, S. & Ben Amar, R. 2013 Emulsion separation using hydrophobic grafted ceramic membranes by. *Colloids and Surfaces A: Physicochemical and Engineering Aspects* **436**, 402–407.

Khemakhem, M., Khemakhem, S. & Amar, R. B. 2014 Surface modification of microfiltration ceramic membrane by fluoroalkylsilane. *Desalination and Water Treatment* **52** (7–9), 1786–1791.

Kim, K. J. & Jang, A. 2016 Fouling characteristics of NOM during the ceramic membrane microfiltration process for water treatment. *Desalination and Water Treatment* **57** (19), 9034–9042.

Kljajević, L. M., Nenadović, S. S., Nenadović, M. T., Bundaleski, N. K., Todorović, B. Ž., Pavlović, V. B. & Rakočević, Z. L. 2017 Structural and chemical properties of thermally treated geopolymer samples. *Ceramics International* **43** (9), 6700–6708.

Konijn, B. J., Sanderink, O. B. J. & Kruyt, N. P. 2014 Experimental study of the viscosity of suspensions: effect of solid fraction, particle size and suspending liquid. *Powder Technology* **266**, 61–69.

Krajewski, S. R., Kujawski, W., Bukowska, M., Picard, C. & Larbot, A. 2006 Application of fluoroalkylsilanes (FAS) grafted ceramic membranes in membrane distillation process of NaCl solutions. *Journal of Membrane Science* **281** (1–2), 253–259.

Kujawa, J., Kujawski, W., Koter, S., Jarzynka, K., Rozicka, A., Bajda, K. & Larbot, A. 2013 Membrane distillation properties of TiO_2 ceramic membranes modified by perfluoroalkylsilanes. *Desalination and Water Treatment* **51** (7–9), 1352–1361.

Kujawa, J., Cerneaux, S., Koter, S. & Kujawski, W. 2014a Highly efficient hydrophobic titania ceramic membranes for water desalination. *ACS Applied Materials & Interfaces* **6** (16), 14223–14230.

Kujawa, J., Cerneaux, S. & Kujawski, W. 2014b Investigation of the stability of metal oxide powders and ceramic membranes grafted by perfluoroalkylsilanes. *Colloids and Surfaces A: Physicochemical and Engineering Aspects* **443**, 109–117.

Kujawa, J., Cerneaux, S. & Kujawski, W. 2014c Characterization of the surface modification process of Al_2O_3, TiO_2 and ZrO_2 powders by PFAS molecules. *Colloids and Surfaces A: Physicochemical and Engineering Aspects* **447**, 14–22.

Kujawa, J., Cerneaux, S., Kujawski, W., Bryjak, M. & Kujawski, J. 2016 How to functionalize ceramics by perfluoroalkylsilanes for membrane separation process? Properties and application of hydrophobized ceramic membranes. *ACS Applied Materials & Interfaces* **8** (11), 7564–7577.

Kujawa, J., Cerneaux, S., Kujawski, W. & Knozowska, K. 2017 Hydrophobic ceramic membranes for water desalination. *Applied Sciences* **7** (4), 402.

Kumari, U., Swamy, K., Gupta, A., Karri, R. R., Meikap, B. C., Dehghani, M. H., Karri, R. & Lima, E. 2021 Global water challenge and future perspective. In: *Green Technologies for the Defluoridation of Water*. Elsevier, Amsterdam, pp. 197–212.

Lee, J. G., Kim, Y. D., Kim, W. S., Francis, L., Amy, G. & Ghaffour, N. 2015 Performance modeling of direct contact membrane distillation (DCMD) seawater desalination process using a commercial composite membrane. *Journal of Membrane Science* **478**, 85–95.

Li, X., Chou, S., Wang, R., Shi, L., Fang, W., Chaitra, G., Tang, C. Y., Torres, J., Hu, X. & Fane, A. G. 2015 Nature gives the best solution for desalination: aquaporin-based hollow fiber composite membrane with superior performance. *Journal of Membrane Science* **494**, 68–77.

Li, H., Liu, Y., Liu, Y., Zeng, Q., Wang, J., Hu, K., Lu, Z. & Liang, J. 2020a Evolution of the microstructure and mechanical properties of stereolithography formed alumina cores sintered in vacuum. *Journal of the European Ceramic Society* **40** (14), 4825–4836.

Li, H., Liu, Y., Liu, Y., Hu, K., Lu, Z. & Liang, J. 2020b Influence of sintering temperature on microstructure and mechanical properties of Al_2O_3 ceramic via 3D stereolithography. *Acta Metallurgica Sinica (English Letters)* **33** (2), 204–214.

Li, B., Yun, Y., Wang, M., Li, C., Yang, W., Li, J. & Liu, G. 2021 Superhydrophobic polymer membrane coated by mineralized β-FeOOH nanorods for direct contact membrane distillation. *Desalination* **500**, 114889.

Lim, S. J. & Shin, I. H. 2020 Graft copolymerization of GMA and EDMA on PVDF to hydrophilic surface modification by electron beam irradiation. *Nuclear Engineering and Technology* **52** (2), 373–380.

Liu, F., Tao, M. m. & Xue, L. x. 2012 PVDF membranes with inter-connected pores prepared via a Nat-ips process. *Desalination* **298**, 99–105.

Liu, Z., Lian, W., Liu, Y., Zhu, J., Xue, C., Yang, Z. & Lin, X. 2021 Phase formation, microstructure development, and mechanical properties of kaolin-based mullite ceramics added with Fe_2O_3. *International Journal of Applied Ceramic Technology* **18** (3), 1074–1081.

Lu, J., Yu, Y., Zhou, J., Song, L., Hu, X. & Larbot, A. 2009 FAS grafted superhydrophobic ceramic membrane. *Applied Surface Science* **255** (22), 9092–9099.

Luo, A. & Lior, N. 2017 Study of advancement to higher temperature membrane distillation. *Desalination* **419**, 88–100.

Magalhaes, F. D. S., Ferreira, E. D. P., Bessa, L. P., Dias, C. C. S., Vieira, A. G. M. & Reis, M. H. M. 2020 Fabrication of kaolin hollow fibre membranes for bacteria removal. *Processing and Application of Ceramics* **14** (4), 303–313.

Mahmoudi, F., Akbarzadeh, A. & Gude, V. G. 2018 Sustainable desalination by permeate gap membrane distillation technology. In: *Emerging Technologies for Sustainable Desalination Handbook*. Butterworth-Heinemann, Elsevier Inc., pp. 157–204.

Mankai, S., Madiouli, J., Sghaier, J. & Lecomte, D. 2018 Determination of porosity from shrinkage curves during sintering of granular materials. *Drying Technology* **36** (5), 557–566.

Merabtene, M., Kacimi, L. & Clastres, P. 2019 Elaboration of geopolymer binders from poor kaolin and dam sludge waste. *Heliyon* **5** (6), e01938.

Mohamed Bazin, M., Ahmad, N. & Nakamura, Y. 2019 Preparation of porous ceramic membranes from Sayong ball clay. *Journal of Asian Ceramic Societies* **7** (4), 417–425.

Mohtor, N. H., Othman, M. H. D., Ismail, A. F., Rahman, M. A., Jaafar, J. & Hashim, N. A. 2017 Investigation on the effect of sintering temperature on kaolin hollow fibre membrane for dye filtration. *Environmental Science and Pollution Research* **24** (19), 15905–15917.

Mouiya, M., Bouazizi, A., Abourriche, A., El Khessaimi, Y., Benhammou, A., Taha, Y. & Hannache, H. 2019 Effect of sintering temperature on the microstructure and mechanical behavior of porous ceramics made from clay and banana peel powder. *Results in Materials* **4**, 100028.

Nafey, A. S., Fath, H. E. S. & Mabrouk, A. A. 2006 A new visual package for design and simulation of desalination processes. *Desalination* **194** (1–3), 281–296.

Ndjigui, P. D., Mbey, J. A., Fadil-Djenabou, S., Onana, V. L., Bayiga, E. C., Enock Embom, C. & Ekosse, G. I. 2021 Characteristics of kaolinitic raw materials from the Lokoundje River (Kribi, Cameroon) for ceramic applications. *Applied Sciences* **11** (13), 6118.

Ni, D. W., Esposito, V., Schmidt, C. G., Molla, T. T., Andersen, K. B., Kaiser, A., Ramousse, S. & Pryds, N. 2013 Camber evolution and stress development of porous ceramic bilayers during co-firing. *Journal of the American Ceramic Society* **96** (3), 972–978.

Obada, D. O., Dodoo-Arhin, D., Dauda, M., Anafi, F. O., Ahmed, A. S. & Ajayi, O. A. 2017a Physico-mechanical and gas permeability characteristics of kaolin based ceramic membranes prepared with a new pore-forming agent. *Applied Clay Science* **150**, 175–183.

Obada, D. O., Dodoo-Arhin, D., Dauda, M., Anafi, F. O., Ahmed, A. S. & Ajayi, O. A. 2017b The impact of kaolin dehydroxylation on the porosity and mechanical integrity of kaolin based ceramics using different pore formers. *Results in Physics* **7**, 2718–2727.

Paiman, S. H., Rahman, A. A. M., Othman, M. H. D. & Ahmad, H. S. 2015 Effect of sintering temperature on the fabrication of ceramic hollow fibre membrane. *ASEAN Journal of Chemical Engineering* **15** (2), 1–10.

Parani, S. & Oluwafemi, O. S. 2021 Membrane distillation: recent configurations, membrane surface engineering, and applications. *Membranes* **11** (12), 934.

Polak, D., Zielińska, I., Szwast, M., Kogut, I. & Małolepszy, A. 2021 Modification of ceramic membranes with carbon compounds for pharmaceutical substances removal from water in a filtration – adsorption system. *Membranes* **11** (7), 481.

Qiu, M., Feng, J., Fan, Y. & Xu, N. 2009 Pore evolution model of ceramic membrane during constrained sintering. *Journal of Materials Science* **44** (3), 689–699.

Qusay, F. A., Ibrahim, S. S. & Khaleel, S. R. 2017 Performance of vacuum poly(propylene) membrane distillation (VMD) for saline water desalination. *Chemical Engineering and Processing: Process Intensification* **120**, 68–80.

Ravi, J., Othman, M. H. D., Matsuura, T., Bilad, M. R. I., El-Badawy, T. H., Aziz, F., Ismail, A. F., Rahman, M. A. & Jaafar, J. 2020 Polymeric membranes for desalination using membrane distillation: a review. *Desalination* **490**, 114530.

Ren, C., Fang, H., Gu, J., Winnubst, L. & Chen, C. 2015 Preparation and characterization of hydrophobic alumina planar membranes for water desalination. *Journal of the European Ceramic Society* **35** (2), 723–730.

Renteria, A., Diaz, J. A., He, B., Renteria-Marquez, I. A., Chavez, L. A., Regis, J. E., Lin, Y., Liu, Y., Espalin, D., Tseng, T. L. B. & Lin, Y. 2019 Particle size influence on material properties of $BaTiO_3$ ceramics fabricated using freeze-form extrusion 3D printing. *Materials Research Express* **6** (11), 115211.

Roy, S. & Ragunath, S. 2018 Emerging membrane technologies for water and energy sustainability: future prospects, constraints and challenges. *Energies* **11** (11), 2997.

Saavedra, A., Valdés, H., Mahn, A. & Acosta, O. 2021 Comparative analysis of conventional and emerging technologies for seawater desalination: Northern Chile as a case study. *Membranes* **11** (3), 180.

Sahnoun, R. D. & Baklouti, S. 2013 Characterization of flat ceramic membrane supports prepared with kaolin-phosphoric acid-starch. *Applied Clay Science* **83–84**, 399–404.

Sanmartino, J. A., Khayet, M. & García-Payo, M. C. 2016 *Desalination by Membrane Distillation, Emerging Membrane Technology for Sustainable Water Treatment*. Elsevier Science, Oxford, pp. 77–109.

Saud, I. H., Othman, M. H. D., Hubadillah, S. K., Aziz, M. H. A., Pauzan, M. A. B., Ismail, A. F., Jaafar, J. & Rahman, M. A. 2021 Superhydrophobic ceramic hollow fibre membranes for trapping carbon dioxide from natural gas via the membrane contactor system. *Journal of the Australian Ceramic Society* **57** (3), 705–717.

Shahabadi, S. M. S., Rabiee, H., Seyedi, S. M., Mokhtare, A. & Brant, J. A. 2017 Superhydrophobic dual layer functionalized titanium dioxide/polyvinylidene fluoride-co-hexafluoropropylene (TiO_2/PH) nanofibrous membrane for high flux membrane distillation. *Journal of Membrane Science* **537**, 140–150.

Shim, W. G., He, K., Gray, S. & Moon, I. S. 2015 Solar energy assisted direct contact membrane distillation (DCMD) process for seawater desalination. *Separation and Purification Technology* **143**, 94–104.

Shirazi, M. M. A., Bastani, D., Kargari, A. & Tabatabaei, M. 2013 Characterization of polymeric membranes for membrane distillation using atomic force microscopy. *Desalination and Water Treatment* **51** (31–33), 6003–6008.

Shirazi, M. M. A., Kargari, A. & Tabatabaei, M. 2014 Evaluation of commercial PTFE membranes in desalination by direct contact membrane distillation. *Chemical Engineering and Processing: Process Intensification* **76**, 16–25.

Singh, D. & Sirkar, K. K. 2012 Desalination of brine and produced water by direct contact membrane distillation at high temperatures and pressures. *Journal of Membrane Science* **389**, 380–388.

Souza, M. Y. M. D., Lira, H. D. L., Santana, L. N. D. L. & Rodríguez, M. A. 2021 Preparation and application in crude oil-water separation of clay-based membranes. *Materials Research* **24** (4).

Subrahmanya, T. M., Lin, P. T., Chiao, Y. H., Widakdo, J., Chuang, C. H., Rahmadhanty, S. F. & Hung, W. S. 2021 High performance self-heated membrane distillation system for energy efficient desalination process. *Journal of Materials Chemistry A* **9** (12), 7868–7880.

Tai, Z. S., Othman, M. H. D., Mustafa, A., Ravi, J., Wong, K. C., Koo, K. N., Hubadillah, S. K., Azali, M. A., Alias, N. H., Ng, B. C., Dzahir, M. I. H. M., Ismail, A. F., Rahman, M. A. & Jaafar, J. 2021 Development of hydrophobic polymethylhydrosiloxane/tetraethylorthosilicate (PMHS/TEOS) hybrid coating on ceramic membrane for desalination via membrane distillation. *Journal of Membrane Science* **637**, 119609.

Twibi, M. F., Othman, M. H. D., Hubadillah, S. K., Alftessi, S. A., Adam, M. R. B., Ismail, A. F., Rahman, M. A., Jaafar, J., Raji, Y. O., Abd, Aziz, M. H., Sokri, M. N. B. M., Abdullah, H. & Naim, R. 2021 Hydrophobic mullite ceramic hollow fibre membrane (Hy-MHFM) for seawater desalination via direct contact membrane distillation (DCMD). *Journal of the European Ceramic Society* **41** (13), 6578–6585.

Usman, J., Othman, M. H. D., Ismail, A. F., Rahman, M. A., Jaafar, J., Raji, Y. O., Gbadamosi, A. O., El Badawy, T. H. & Said, K. A. M. 2021 An overview of superhydrophobic ceramic membrane surface modification for oil-water separation. *Journal of Materials Research and Technology* **12**, 643–667.

Vasanth, D., Uppaluri, R. & Pugazhenthi, G. 2011 Influence of sintering temperature on the properties of porous ceramic support prepared by uniaxial dry compaction method using low-cost raw materials for membrane applications. *Separation Science and Technology* **46** (8), 1241–1249.

Wang, T., Zhang, Y., Li, G. & Li, H. 2009 Preparation and characterization of alumina hollow fiber membranes. *Frontiers of Chemical Engineering in China* **3** (3), 265–271.

Wang, J. W., Li, L., Zhang, J. W., Xu, X. & Chen, C. S. 2016 β-Sialon ceramic hollow fiber membranes with high strength and low thermal conductivity for membrane distillation. *Journal of the European Ceramic Society* **36** (1), 59–65.

Wang, M., Liu, G., Yu, H., Lee, S. H., Wang, L., Zheng, J. & Lee, J. K. 2018 ZnO nanorod array modified PVDF membrane with superhydrophobic surface for vacuum membrane distillation application. *ACS Applied Materials & Interfaces* **10** (16), 13452–13461.

Yang, Z. & Tang, C. Y. 2018 *Novel Membranes and Membrane Materials, Membrane-Based Salinity Gradient Processes for Water Treatment and Power Generation*. Elsevier B.V., Swansea, UK, pp. 201–221.

Yang, Y., Liu, Q., Wang, H., Ding, F., Jin, G., Li, C. & Meng, H. 2017 Superhydrophobic modification of ceramic membranes for vacuum membrane distillation. *Chinese Journal of Chemical Engineering* **25** (10), 1395–1401.

Zewdie, T. M., Habtu, N. G., Dutta, A. & Van der Bruggen, B. 2021a Solar-assisted membrane technology for water purification: a review. *Journal of Water Reuse and Desalination* **11** (1), 1–32.

Zewdie, T. M., Prihatiningtyas, I., Dutta, A., Habtu, N. G. & Van der Bruggen, B. 2021b Characterization and beneficiation of Ethiopian kaolin for use in fabrication of ceramic membrane. *Materials Research Express* **8** (11), 115201.

Zhang, J., Gray, S. & Li, J. D. 2013 Predicting the influence of operating conditions on DCMD flux and thermal efficiency for incompressible and compressible membrane systems. *Desalination* **323**, 142–149.

Zhang, J. W., Fang, H., Wang, J. W., Hao, L. Y., Xu, X. & Chen, C. S. 2014 Preparation and characterization of silicon nitride hollow fiber membranes for seawater desalination. *Journal of Membrane Science* **450**, 197–206.

Zhou, J., Zhang, X., Wang, Y., Larbot, A. & Hu, X. 2010 Elaboration and characterization of tubular macroporous ceramic support for membranes from kaolin and dolomite. *Journal of Porous Materials* **17** (1), 1–9.

Zulfiqar, F., Zubair, M., Ullah, R., Sharma, S., Inoue, M., Asghar, S. & Shivakoti, G. 2021 Climate-induced water scarcity and the effectiveness of community-based water resource management. *Natural Resource Governance in Asia* **22**, 343–351.

Zulkifli, S. N. A., Mustafa, A., Othman, M. H. D. & Hubadillah, S. K. 2020 Fabrication and characterisation of hollow fibre ceramic membranes from fly ash. *Malaysian Journal of Fundamental and Applied Sciences* **16** (5), 508–513.

Zuo, J. & Chung, T. S. 2016 Metal-organic framework-functionalized alumina membranes for vacuum membrane distillation. *Water* **8** (12), 1–15.

First received 19 December 2021; accepted in revised form 25 February 2022. Available online 10 March 2022